Received: 2 June 2022 | Accepted: 18 July 2022

DOI: 10.1002/maco.202213329

ARTICLE

Materials and Corrosion

High temperature corrosion behavior of alloys in reducing HCl and H2S containing environments: Thermodynamical and experimental assessment

Manuela Nimmervoll[1] | **Gregor Mori**[1] | **Edith Bucher**[1] | **Stefan Hönig**[2] | **Roland Haubner**[3]

[1]Montanuniversität Leoben, Leoben, Austria

[2]OMV E&P GmbH, Gänserndorf, Austria

[3]Technische Universität Wien, Vienna, Austria

Correspondence
Manuela Nimmervoll, Montanuniversität Leoben, A-8700 Leoben, Austria.
Email: manuela.nimmervoll@omv.com

Abstract

High-temperature corrosion mechanisms in reducing atmospheres containing HCl (3.8 vol%) and a varying amount of H_2S (0.02 –2 vol%) were developed for several alloys between 420°C and 680°C. These mechanisms are mainly based on practical observations and kinetic considerations—and less on thermodynamic data. This is due to the complexity of these mixed gas atmospheres, volatile corrosion products, and the ever-changing conditions within the corrosion layer, which made it not possible to predict and calculate the actual conditions in the corrosion zone. In this article, a detailed thermodynamic analysis of previously achieved corrosion mechanisms and experimental observations is presented. Correlations and deviations between thermodynamic calculations and practical findings are stated and discussed. The corrosion behavior of ferritic K90941, which performs worse than corrosion-resistant austenitic alloys, except for one test condition at 580°C in the atmosphere with 0.2 vol% H_2S, is explained and supported by thermodynamic data. By combining experiments with thermodynamics, corrosion mechanisms in reducing HCl and H2S-containing atmospheres are explained.

KEYWORDS

corrosion mechanism, H_2S, HCl, high temperature corrosion, thermodynamics, volatile corrosion products

1 | INTRODUCTION

Thermal cracking of plastic waste is a promising chemical recycling alternative to mechanical recycling routes. During the thermal cracking of plastic waste, the macromolecular hydrocarbon structures of the polymers are broken down into smaller monomeric units. Thereby, raw materials for petrochemical processes or feedstock that can be used to produce monomers or other valuable hydrocarbons, with similar qualities to those of conventional substances, can be generated.[1–3]

One major problem during thermal cracking of plastic waste is the rather unpredictable specification of the plastic feedstock, especially for waste materials of unknown origin and formulation. Impurities inside of the feedstock, like chlorine-containing plastics or biological contaminations, can lead to the formation of HCl or H_2S, respectively, during the cracking process. These two gases are known to cause high-temperature corrosion of metallic materials.[1,2,4–6] Thus, conditions that form in the reactor zone during the thermal decomposition of plastic waste are reducing and are expected to contain several corrosive agents. Besides sulfidation also the formation of volatile corrosion products is possible. In both cases, the formed corrosion scales are loose and nonprotective. A severe corrosive attack of the alloys is the consequence.[5,7–17]

These complex and mixed gas atmospheres are challenging for the prediction of the high-temperature corrosion behavior of alloys due to a variety of several interacting and simultaneous occurring chemical reactions. In contrast to many fundamental processes of high-temperature corrosion that are nowadays understood, for complex technical atmospheres and sophisticated technical materials, this knowledge can only be used to make approaches and to interpret observed tendencies.[6,18–25] Thus, there is still a strong need for intensive research in the field of high-temperature corrosion, based on experimental investigations, to describe the actual behavior of the materials and the corrosion mechanisms behind this.

In several cases, thermodynamic data can help to understand and describe corrosion mechanisms. Equilibrium calculations can be a useful tool for the prediction of which chemical reactions may take place during a corrosion process by determining the most stable state of the reacting system. The change in Gibbs free energy ΔG^0 is therefore helpful to analyze corrosion reactions. If the change of ΔG^0 is negative for a corrosion reaction, the reaction occurs spontaneously and the reaction can take place.[23,26–28]

In complex atmospheres, with more than one reactive gaseous compound, these thermodynamic calculations have to be performed for all relevant reaction partners, which can form a corrosion product. The calculated results can be illustrated in isothermal phase stability diagrams. Phase stability diagrams can also be applied if a material consists of various alloying elements, in which each element can react with the surrounding atmosphere to form different corrosion products. It should be emphasized that these diagrams are only thermodynamical reflections and do not consider kinetic effects. Another drawback of phase stability diagrams is that interactions between three or more gaseous species are excluded since the diagrams are only two-dimensional. Nevertheless, they are helpful for first estimations of the type of material that may show protective behavior in a particular atmosphere.[23,27,28]

The high-temperature corrosion behavior in reducing HCl and H_2S containing atmospheres of several alloys, ranging from low-alloyed ferritic K90941 up to highly alloyed austenitic N10276, was investigated at various conditions during previous studies[6,18–22,24,25,29,30] and different corrosion models were generated.[18,20,24,25] In Table 1, an overview of all performed experiments in reducing HCl and H2S-containing atmospheres is presented and corresponding references to the published results are denoted. A detailed analysis of these results can be found in the respective references. The main challenge in developing the corrosion mechanisms was the overall chemistry, including thermodynamics, kinetics, diffusion, and so on, due to a variety of possible

TABLE 1 Overview of performed tests (parameters: material, atmosphere, temperature) with the mark "x" showing that experiments were executed

	Low-H_2S				Mid-H_2S			High-H_2S		
Material	**420°C**	**480°C**	**580°C**	**680°C**	**420°C**	**480°C**	**580°C**	**420°C**	**480°C**	**580°C**
K90941	x[21]	x[29]	x[21,29]	x[19,29]	x	x	x	x[21]	x	x[21]
S30403	x[25]	x[25]	x[25]		x[25]	x[25]	x[25]	x[25]	x[25]	x[25]
S31603	x[25]	x[25]	x[25]		x[25]	x[25]	x[25]	x[25]	x[25]	x[25]
S32205		x[6,29]	x[6,29]	x[6,19,22,29]						
S30815	x[25]	x[25]	x[25]		x[25]	x[25]	x[25]	x[25]	x[25]	x[25]
S31400		x[6,20,29]	x[6,29]	x[6,18,19,29,30]						
S31008	x[25]	x[25]	x[25]		x[25]	x[25]	x[25]	x[25]	x[25]	x[25]
N08811	x[21,25]	x[20,25,29]	x[21,25,29]	x[19,29]	x[25]	x[25]	x[25]	x[21,25]	x[25]	x[21,25]
N06600		x[20,29]	x[29]	x[19,20,29]						
N10276		x[24]	x	x[19,24]						

Note: Composition of low-H2S, mid-H2S, and high-H2S gas mixture can be found in Table 3.

chemical reactions and no data available for the actual corrosion zone. In this article, a detailed thermodynamic analysis of previously achieved experimental results is presented and the approach that is used to achieve the corrosion mechanisms is explained in detail.

2 | EXPERIMENTAL METHODS AND MATERIALS

From a collection of recently achieved experimental results and in combination with detailed thermodynamic analysis, an overall concept of corrosion mechanisms in reducing HCl and H2S-containing atmospheres was developed. Therefore, thermodynamic calculations are discussed on the basis of results of the ferritic material K90941 and of results of the austenitic materials S30403, S31603, S30815, S31008, and N08811, which were already published in a previous study.[25] The chemical compositions of the alloys are shown in Table 2.

The corrosion experiments were done to evaluate the material behavior under process conditions simulating a thermal cracking process of waste plastics. The tests were performed at 420°C, 480°C, and 580°C in lab-scale test equipment consisting of a silica glass tube, in which the samples were placed. After purging with N_2, the assembly was heated up by a tube furnace and then the HCl and H_2S containing the gas mixture were induced. A detailed explanation of the setup of the test equipment can be found in previous studies and is not the subject of this article.[6,20]

The test gas mixtures, which were used for the experiments, consisted of a varying amount of H_2S (0.02 , 0.2, or 2 vol%) and 3.8 vol% HCl, 1.9 vol% CO_2, 0.3 vol% CO, 2.8 vol% H_2, bal. N_2, representing possible atmospheres of a thermal cracking process of waste plastics. The different gas mixtures are denoted as a low-H_2S mixture, mid-H_2S mixture, and high-H_2S mixture, respectively. The exact gas compositions are listed in Table 3.

After the experiments, metallographic cross-sections of the corroded materials were prepared for scanning electron microscopy-energy dispersive X-ray (SEM/EDX) investigations (Zeiss, EVO MA 25®, LaB_6 cathode, samples sputtered with gold). Loose corrosion products were characterized by X-ray diffraction analysis (XRD) (PanAlytical X'Pert Pro diffractometer, Bragg-Brentano geometry, $CuK_{\alpha 1,2}$ radiation, X'Celerator multi-channel detector, zero-background silicon sample holder, scan length 2.546°, 2θ range 5-70°, 10 s exposure time per scan length). The mass loss was determined by removing the corrosion products with 5% hydrochloric acid and a wire brush. A detailed experimental procedure can be found in previous studies and is not the subject of this article.[6,20]

Several thermodynamic calculations for the different test conditions were done with the software Fact Sage 8.0. The method of the thermodynamic equilibrium calculations is based on the minimization of Gibbs free energy in a closed and homogeneous system. Chemical equilibrium can be calculated if a system is defined in terms of temperature, pressure (or volume), enthalpy, and equilibrium activities of any phase in the system. As a result, the amounts of all stable phases, which reach a state of chemical equilibrium, are given as a function of temperature.[26,31] Thereby, equilibrium calculations of the initial gas mixtures were performed, receiving partial pressures of all gas species that will be thermodynamically established. In addition, equilibrium calculations of the initial gas mixtures with consideration of the three main metals (Fe, Cr, Ni) were performed for all conditions, assuming an excess amount of metal of 1000 mole. With this method, all solid reaction products (activity = 1), as well as partial pressures of important volatile reaction products, could be predicted. Moreover, several calculations about Gibbs free energy of reaction were performed to assess, which reactions are most favored. In addition to thermodynamic calculations, quasi-stability diagrams for the systems Me–S–O–Cl were created according to the concept of Bender, Schütze, and Schwalm.[5,32]

TABLE 2 Chemical composition of the tested materials in [wt%]

Material	Fe	Ni	Cr	C	Mn	Si	Mo	Ti	Al
K90941	89	-	9	0.10	0.5	0.5	1	-	-
S30403	70	10	18.3	0.01	1.2	0.4	0.3	-	-
S31603	69	10.2	16.8	0.01	1.8	0.3	2	-	-
S30815	66	11	21	0.08	0.8	1.5	-	-	-
S31008	50.5	21	25	0.03	2	1.5	-	-	-
N08811	47.5	30.4	20.5	0.07	0.6	-	-	0.5	0.5

TABLE 3 Composition of the test gas atmospheres in [vol%]

Gas nomenclature	H_2S	HCl	CO	CO_2	H_2	N_2
Low-H_2S	0.02	3.8	0.3	1.9	2.8	bal.
Mid-H_2S	0.2	3.8	0.3	1.9	2.8	bal.
High-H_2S	2	3.8	0.3	1.9	2.8	bal.

3 | RESULTS AND DISCUSSION

3.1 | Thermodynamic evaluation

In general, thermodynamics is able to predict which reaction products are in equilibrium with a defined environment at a certain temperature. It can help to estimate the formation of corrosion products. For thermodynamic assessment of the corrosion behavior of alloys in reducing HCl and H2S-containing environments, equilibrium calculations of the gas mixtures with and without consideration of the base metals, as well as calculations about free energies of reaction were performed. However, these calculations consider only thermodynamic equilibrium states of reactions, whereas none beyond these equilibrium states is captured. In addition, thermodynamics is not able to predict the rate of corrosion reactions, which is part of kinetics.[33]

3.1.1 | Equilibrium calculations of the gas mixtures

To evaluate the partial pressures of corrosive species formed in the different tested gas atmospheres, thermodynamic equilibrium calculations for the initial gas mixtures (Table 3) were performed. As a first step, these calculations were done without the consideration of the reaction with metals and only for the gas environments themselves. In Table 4 most relevant partial pressures, which will arise in the initial gas mixtures are listed. Partial pressures of H_2O, which established in the gas mixtures due to the reverse water gas shift reaction, were added since H_2O was identified to take part in the given corrosion processes.[18]

As shown in Table 4, the three reducing atmospheres produce very similar chlorine and oxygen partial pressures at the same temperatures, while the sulfur pressures differ. The high-H_2S mixture provided the largest sulfur pressure, followed by the mid-H_2S mixture and the low-H_2S mixture. Thus, it could be seen that the subsidizing character was highest in the high-H_2S mixture.

3.1.2 | Equilibrium calculations considering the main metals

Additional thermodynamic equilibrium calculations of the initial gas mixtures considering reactions with the three main metals (Fe, Cr, Ni) were performed for all conditions, assuming an excess amount of metal of 1000 mole. With this method, thermodynamically most stable products are evaluated. Corrosion processes like the sulfidation of metals will occur if the partial pressure of the corrosive sulfur species in the gas atmosphere is greater than the sulfur partial pressure in equilibrium with the sulfide. These formation pressures of the corresponding metal sulfides can be calculated via thermodynamics. The same is applicable to the formation of metal oxides, metal chlorides, and so on.

Calculations of the gas mixtures including all three base metals in one calculation step were considered to be not successful since only reaction products of the most reactive metal (Cr) with the gas phase would be revealed, whereas the less reactive metals (Fe and Ni) would remain in their metallic form. Thus, separate calculations for each metal with every gas mixture were performed. An overview of resulting solid reaction products with an activity equal to one can be found in Table 5. In Table 6 most relevant volatile corrosion products, which will form during reactions of the metal with the gas mixture, and their calculated partial pressures for $p \geq 10^{-15}$ bar are listed. These vapor pressures account for the whole gas mixture and not only for the reaction of metal with the individual gas species. Table 6 can present a helpful

TABLE 4 Partial pressures of most relevant gas components of the given atmospheres (initial conditions) at different temperatures in [bar] without consideration of the main metals (calculated by FactSage 8.1)

	420°C			480°C			580°C		
Gas species	Low-H_2S	Mid-H_2S	High-H_2S	Low-H_2S	Mid-H_2S	High-H_2S	Low-H_2S	Mid-H_2S	High-H_2S
S_2	8.9×10^{-13}	8.9×10^{-11}	8.9×10^{-09}	5.4×10^{-12}	5.4×10^{-10}	5.4×10^{-08}	1.2×10^{-10}	1.2×10^{-08}	1.2×10^{-06}
Cl_2	1.5×10^{-16}	1.5×10^{-16}	1.5×10^{-16}	1.4×10^{-15}	1.4×10^{-15}	1.4×10^{-15}	4.2×10^{-14}	4.2×10^{-14}	4.2×10^{-14}
O_2	2.2×10^{-32}	2.2×10^{-32}	2.2×10^{-32}	5.0×10^{-30}	5.1×10^{-30}	5.1×10^{-30}	3.6×10^{-26}	3.6×10^{-26}	3.6×10^{-26}
H_2S	2.0×10^{-04}	2.0×10^{-03}	2.0×10^{-02}	2.0×10^{-04}	2.0×10^{-03}	2.0×10^{-02}	2.0×10^{-04}	2.0×10^{-03}	2.0×10^{-02}
HCl	3.8×10^{-02}	3.8×10^{-02}	3.8×10^{-02}	3.8×10^{-02}	3.8×10^{-02}	3.8×10^{-02}	3.8×10^{-02}	3.8×10^{-02}	3.8×10^{-02}
CO	1.6×10^{-03}	1.6×10^{-03}	1.6×10^{-03}	5.2×10^{-03}	5.2×10^{-03}	5.2×10^{-03}	1.0×10^{-02}	1.0×10^{-02}	1.0×10^{-02}
CO_2	1.4×10^{-02}	1.4×10^{-02}	1.4×10^{-02}	1.4×10^{-02}	1.4×10^{-02}	1.4×10^{-02}	1.1×10^{-02}	1.1×10^{-02}	1.1×10^{-02}
H_2	1.3×10^{-02}	1.3×10^{-02}	1.3×10^{-02}	1.8×10^{-02}	1.8×10^{-02}	1.8×10^{-02}	2.0×10^{-02}	2.0×10^{-02}	2.0×10^{-02}
H_2O	1.1×10^{-02}	1.1×10^{-02}	1.1×10^{-02}	7.9×10^{-03}	8.0×10^{-03}	8.0×10^{-03}	7.5×10^{-03}	7.5×10^{-03}	7.6×10^{-03}

TABLE 5 Calculated corrosion products (solid) with activity = 1

Low- H_2S			Mid- H_2S			High- H_2S		
420°C	480°C	580°C	420°C	480°C	580°C	420°C	480°C	580°C
Cr	Cr	Cr	Cr	Cr	Cr	Cr	Cr	Cr
Cr_2N	Cr_2N	Cr_2N	Cr_2N	Cr_2N	Cr_2N	Cr_2N	Cr_2N	Cr_2N
$CrCl_2$	$CrCl_2$	$CrCl_2$	$CrCl_2$	$CrCl_2$	$CrCl_2$	$CrCl_2$	$CrCl_2$	$CrCl_2$
Cr_2O_3	Cr_2O_3	Cr_2O_3	Cr_2O_3	Cr_2O_3	Cr_2O_3	Cr_2O_3	Cr_2O_3	Cr_2O_3
CrS	CrS	CrS	CrS	CrS	CrS	CrS	CrS	CrS
Fe	Fe	Fe	Fe	Fe	Fe	Fe	Fe	Fe
$FeCl_2$	$FeCl_2$	$FeCl_2$	$FeCl_2$	$FeCl_2$	$FeCl_2$	$FeCl_2$	$FeCl_2$	$FeCl_2$
Fe_3O_4	Fe_3O_4	FeO	Fe_3O_4	Fe_3O_4	FeO	Fe_3O_4	Fe_3O_4	FeO
FeS	FeS	FeS	FeS	FeS	FeS	FeS	FeS	FeS
Ni	Ni	Ni	Ni	Ni	Ni	Ni	Ni	Ni
$NiCl_2$	-	-	$NiCl_2$	-	-	-	-	-
Ni_3S_2	Ni_3S_2	Ni_3S_2	Ni_3S_2	Ni_3S_2	Ni_3S_2	Ni_3S_2	Ni_3S_2	Ni_3S_2

Note: Obtained from thermodynamic equilibrium calculations of the different H2S-mixtures considering the three main metals Cr, Fe, Ni (for each metal Cr, Fe, Ni separately calculated) assuming excess metal (1000 mole) at different temperatures.

TABLE 6 Calculated corrosion products (gaseous) with corresponding vapor pressures down to 10^{-15}bar

420°C		480°C		580°C	
Product	Vapor pressure [bar]	Product	Vapor pressure [bar]	*Product*	Vapor pressure [bar]
$FeCl_2$	10^{-06}	$FeCl_2$	10^{-05}	$FeCl_2$	10^{-04}
$NiCl_2$	10^{-08}	$(FeCl_2)_2$	10^{-07}	$(FeCl_2)_2$	10^{-05}
$(FeCl_2)_2$	10^{-08}	$NiCl_2$	10^{-08}	$NiCl_2$	10^{-07}
$FeCl_3$	10^{-11}	$CrCl_2$	10^{-09}	$CrCl_2$	10^{-07}
$CrCl_2$	10^{-11}	$FeCl_3$	10^{-09}	$FeCl_3$	10^{-07}
$CrCl_3$	10^{-14}	$CrCl_3$	10^{-13}	$CrCl_3$	10^{-10}
$Fe(OH)_2$	10^{-15}	$Fe(OH)_2$	10^{-14}	CrCl	10^{-11}
		CrCl	10^{-14}	$Fe(OH)_2$	10^{-12}
		NiCl	10^{-15}	NiCl	10^{-13}
		-	-	$Fe(Cl_3)_2$	10^{-13}

Note: Products are equal for all gas mixtures irrespective of H2S content. Obtained from thermodynamic equilibrium calculations of the different H2S-mixtures considering the three main metals Cr, Fe, Ni (for each metal Cr, Fe, Ni separately calculated) assuming excess metal (1000 mole) at different temperatures.

indication to estimate the possible volatilization of different metal chlorides and other volatile species.

Comparing the predicted phases of the different H_2S-mixtures in Table 5, no differences between formed corrosion products are visible, except that the formation of $NiCl_2$ is only predicted at 420°C in the low- and the mid-H_2S mixture. At all other conditions, $NiCl_2$ is thermodynamically not expected. Comparing the calculated vapor pressures of volatile corrosion products (Table 6), it can be seen that vapor pressures differ between the temperature, but not between the gas mixtures when excess metal (1000 mole) is used in the calculation. With the rising temperature, the vapor pressure of the individual products also increased, and overall more volatile species are present in the gas phase down to a defined vapor pressure (in Table 6 down to 10^{-15} bar). Thus, with the data of Tables 5 and 6, a similar corrosion behavior would be expected in the three atmospheres regarding the formation of solid and volatile corrosion products depending only on temperature.

3.1.3 | Gibbs free energy of reaction

As thermodynamic equilibrium calculations considered the main metals (Cr, Fe, Ni) separately, it was also of interest, which reactions preferentially will take place. Thus, calculations of Gibbs free energy of reaction of several reactions were performed and calculated Δ_rG^0 values are given in Table 7.

Since the formation of metal chlorides was predicted, the reaction of the base metal with HCl is assumed. As can be seen in Table 7, in the case of reactions of HCl with the three main metals, the reaction with Cr shows the most negative Δ_rG^0 value indicating that this reaction will take place preferentially, followed by iron. Nickel even shows a positive Δ_rG^0 value, thus it can be assumed that the reaction of nickel with HCl will only take place to a very small amount as the equilibrium of the reaction is on the educts side. The reactions of the main metals with H_2S also revealed the most negative Δ_rG^0 values for the reaction of chromium with H_2S indicating that this metal will be preferentially attacked and form the corresponding sulfides.

In addition to reactions of HCl and H_2S with the base metals, also the reactions of volatile metal chlorides with H_2S were considered. According to Δ_rG^0 values for these reactions, first $NiCl_2$ would react to form nickel sulfide and then $FeCl_2$ and $CrCl_2$. But since $NiCl_2$ is expected to be the least available metal chloride, it is hard to predict which reactions will dominate. This is illustrated in Figure 1, where respective Δ_rG^0 values are plotted versus temperature, which will be discussed in a later section.

Nevertheless, due to the variety of possible chemical reactions, it is not possible to forecast which reactions will take place to what extent. Thus, to identify which corrosion products might actually form, experimental data are needed.

TABLE 7 Δ_rG^0 values of several possible reactions in [J]

Chemical reaction		$\Delta_rG°$[J]		
		420°C	480°C	580°C
1	$Fe + 2\ HCl \rightarrow FeCl_2 + H_2$	**−55878**	**−47913**	**−34808**
2	$Ni + 2\ HCl \rightarrow NiCl_2 + H_2$	**−2608**	6932	22634
3	$Cr + 2\ HCl \rightarrow CrCl_2 + H_2$	**−109769**	**−101822**	**−88812**
4	$Fe + H_2S \rightarrow FeS + H_2$	**−62719**	**−62152**	**−61302**
5	$Fe + 2\ H_2S \rightarrow FeS_2 + 2\ H_2$	**−48981**	**−42892**	**−32899**
6	$Ni + H_2S \rightarrow NiS + H_2$	**−34722**	**−32955**	**−30150**
7	$Ni + 2/3\ H_2S \rightarrow 1/3$ Ni3S2 $+ 2/3\ H_2$	**−35817**	**−34170**	**−32086**
8	$Cr + H_2S \rightarrow CrS + H_2$	**−94551**	**−93528**	**−91972**
9	$Cr + 3/2\ H_2S \rightarrow 1/2\ Cr_2S_3 + 3/2\ H_2$	**−99922**	**−97820**	**−94549**
10	$Cr + 4/3\ H_2S \rightarrow 1/3\ Cr_3S_4 + 4/3\ H_2$	**−96717**	**−94627**	**−91252**
11	$FeCl_2 + H_2S \rightarrow FeS + 2\ HCl$	**−6840**	**−14239**	**−26494**
12	$NiCl_2 + H_2S \rightarrow NiS + 2\ HCl$	**−32114**	**−39887**	**−52784**
13	$CrCl_2 + H_2S \rightarrow CrS + 2\ HCl$	15218	8294	**−3160**
14	$CrCl_2 + 3/2\ H_2S \rightarrow 1/2\ Cr_2S_3 + 2\ HCl + 1/2\ H_2$	9847	4002	**−5737**
15	$CrCl_2 + 4/3\ H_2S \rightarrow 1/3\ Cr_3S_2 + 2\ HCl + 1/3\ H_2$	13052	7195	**−2440**
16	$CO_2 + H_2 \rightarrow CO + H_2O$	13378	11278	7887
17	$FeCl_2 + H_2O \rightarrow FeO + 2\ HCl$	46038	38647	26405
18	$NiCl_2 + H_2O \rightarrow NiO + 2\ HCl$	36074	28627	16248
19	$CrCl_2 + 3/2\ H_2O \rightarrow 1/2\ Cr_2O_3 + 2\ HCl + 1/2\ H_2$	**−48345**	**−53465**	**−61977**
20	$2\ Cr + 1/2\ N_2 \rightarrow Cr_2N$	**−72955**	**−68746**	**−61845**

Note: Bold values show negative Δ_rG^0 values meaning that these reactions can occur spontaneously and can take place.

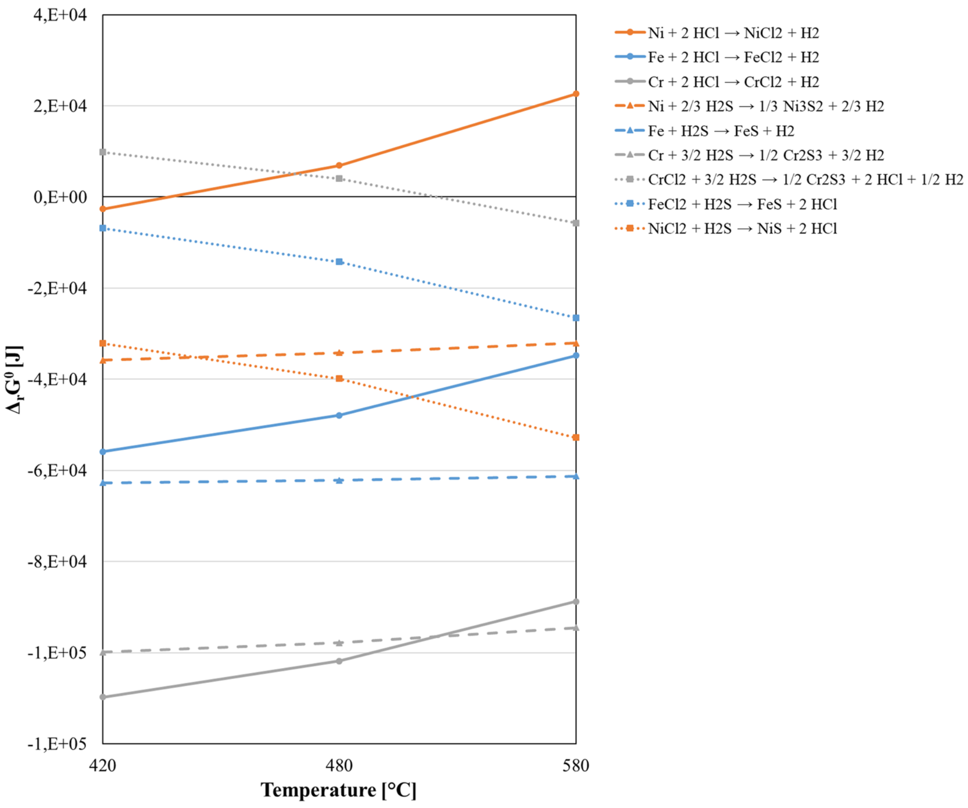

FIGURE 1 Gibbs free energies of selected reactions against temperature [Color figure can be viewed at wileyonlinelibrary.com]

3.1.4 | Quasi-stability diagrams

In addition to the equilibrium calculations, and as a final thermodynamical step, quasi-stability diagrams of the system Me–S_2–Cl_2–O_2 with Me=Fe, Cr, Ni were constructed following the example of Bender, Schütze, and Schwalm.[5,32] With these diagrams the corrosion products that might form under calculated partial pressures of the different test gas atmospheres (Table 4) can be estimated.

Quasi-stability diagrams are based on thermodynamic calculations in combination with the Hertz–Langmuir equation. In contrast to conventional phase-stability diagrams, which only consider solid and liquid phases with $a = 1$, quasi-stability diagrams also include the formation of certain gaseous components above solid or liquid phases. In such diagrams, the partial pressures of chlorine and oxygen under which the partial pressure of the volatile corrosion products reaches 10^{-4} bar are calculated for a constant temperature. At pressures $\geq 10^{-4}$ bar, it is assumed that mass loss due to evaporating metal chlorides is significant. This boundary value, at which the emerging corrosion products' partial pressure reaches 10^{-4} bar, was based on experimental observations and the assumption that all metals react similarly to iron. This value is often considered critical for gaseous corrosion products and a theoretical explanation for it can be found in the Hertz–Langmuir equation.[5,34–36] Quasi-stability diagrams show that the possible risk of chlorine-induced high-temperature corrosion is underestimated. Thus, the diagrams can be a useful tool to assess the potential for the formation of volatile corrosion products.

Quasi-stability diagrams for the system Me–S_2–Cl_2–O_2 (Me=Fe, Cr, Ni) with an indication of the equilibrium partial pressures of the corrosive species for all given gas mixtures were constructed. Figure 2 gives an example of one of those quasi-stability diagrams on the system Fe–S_2–Cl_2–O_2 at 580°C. The different marks in Figure 2 represent the respective partial pressures, which were calculated to be formed in the initial gas mixtures (Table 4). At 580°C, partial pressures of chlorine were calculated for all three mixtures to be in the range of 10^{-14} bar and for oxygen to be around 10^{-26} bar. This explains why in the Fe–O_2–Cl_2 (Figure 2c) system the three marks overlap. However, as can be seen, partial pressures of sulfur differ. The sulfur pressure, which forms in the low-H_2S mixture (represented by the red triangle in Figure 2) was calculated to be the lowest with around 10^{-10} bar. The sulfur partial pressure of the mid-H_2S mixture (represented by the blue circle in Figure 2) laid in the middle with around 10^{-08} bar and the sulfur partial pressure of the high-H_2S mixture (represented by

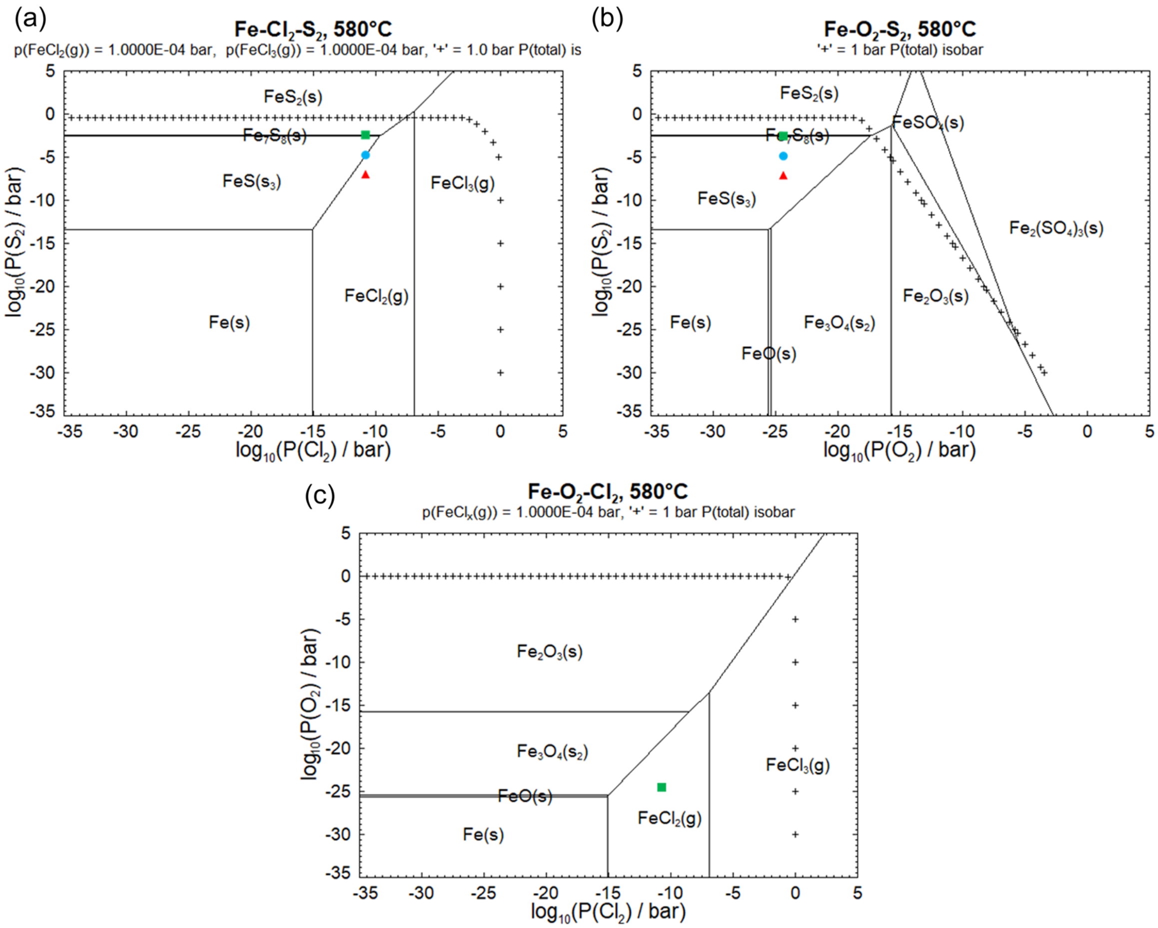

FIGURE 2 Quasi-stability diagrams of the system Fe–S_2–Cl_2–O_2 at 580°C with marks representing the partial pressures of the different mixtures (red triangle = low-H_2S mixture, blue circle = mid-H_2S mixture, green square = high-H_2S mixture), whereby marks in (c) Fe–O_2–Cl_2 are overlapping due to same partial pressures of oxygen and chlorine in all three gas mixtures. [Color figure can be viewed at wileyonlinelibrary.com]

the green square in Figure 2) was calculated to be the highest with around 10^{-06} bar. Therefore, the quasi-stability diagrams estimate for the low-H_2S mixture (red triangle) and the mid-H_2S mixture (blue circle) at 580°C the thermodynamically stable phases $FeCl_2$ and FeS, and for the high-H_2S mixture (green square) the thermodynamically stable phases $FeCl_2$, FeS, and FeS_2. In the case of the mid-H_2S mixture, it can be shown that in the Fe–S_2–Cl_2 diagram the blue circle is on the borderline between $FeCl_2$ and FeS. Thus, it can be assumed that H_2S and HCl compete simultaneously for the predominance of iron and, depending on local shifts of sulfur and chlorine partial pressure due to other reactions, either H_2S or HCl will react with iron.

The other quasi-stability diagrams of the systems Me–S_2–Cl_2–O_2 (Me=Fe, Cr, Ni) at different temperatures can be found in the Supporting Information Material. In Table 8, thermodynamically stable phases according to the quasi-stability diagrams for each system Me–S_2–Cl_2–O_2 are listed. As indicated in Table 8, the tendency to form metal sulfides is largest in the high-H_2S mixture, since also the Fe–S_2–Cl_2 and the Cr–S_2–Cl_2 system reveal the formation of sulfides at all temperatures compared with the low- and mid-H_2S mixtures, where the formation of $FeCl_2$ and $CrCl_2$ is predicted. With regard to volatile species, the Fe–Cl_2–O_2 systems give an indication that gaseous $FeCl_2$ might form from 580°C in all mixtures. Thus, it can be assumed that volatile products play a role in the corrosion processes in the given gas mixtures and that the sulfidizing character of the environment will be the largest in the high-H_2S mixture.

3.1.5 | Consolidation of thermodynamic data and possible corrosion reactions

As partial pressures (Table 4), which are established in the gas mixtures, are much higher for sulfur and chlorine than for oxygen, sulfur, and chlorine-containing gas species, H_2S and HCl, widely determine the corrosion processes. Their individual interactions with the three

TABLE 8 Phases identified in quasi-stability diagrams of several Me–S_2–Cl_2–O_2 systems with partial pressures of S_2, Cl_2, and O_2 calculated from the initial gas mixtures without consideration of main metals (listed in Table 4)

	Low-H_2S			Mid-H_2S			High-H_2S		
System	420°C	480°C	580°C	420°C	480°C	580°C	420°C	480°C	580°C
Fe–S_2–Cl_2	$FeCl_2$(s)	$FeCl_2$(s)	$FeCl_2$(g)	$FeCl_2$(s)/ FeS(s)	$FeCl_2$(s)/ FeS(s)	$FeCl_2$(g)/ FeS(s)	FeS_2(s)	FeS_2(s)	FeS(s)/ FeS_2(s)
Fe–S_2–O_2	FeS(s)	FeS(s)	FeS(s)	FeS(s)	FeS(s)	FeS(s)	FeS_2(s)	FeS_2(s)	FeS(s)/ FeS_2(s)
Fe–Cl_2–O_2	$FeCl_2$(s)	$FeCl_2$(s)	$FeCl_2$(g)	$FeCl_2$(s)	$FeCl_2$(s)	$FeCl_2$(g)	$FeCl_2$(s)	$FeCl_2$(s)	$FeCl_2$(g)
Cr–S_2–Cl_2	$CrCl_2$(s)	$CrCl_2$(s)	$CrCl_2$(s)	$CrCl_2$(s)	$CrCl_2$(s)/ Cr_2S_3(s)	$CrCl_2$(s)/ Cr_2S_3(s)	Cr_2S_3(s)	Cr_2S_3(s)	Cr_2S_3(s)
Cr–S_2–O_2	Cr_2O_3(s)	Cr_2O_3(s)	Cr_2O_3(s)	Cr_2O_3(s)	Cr_2O_3(s)	Cr_2O_3(s)	Cr_2O_3(s)	Cr_2O_3(s)	Cr_2O_3(s)
Cr–Cl_2–O_2	Cr_2O_3(s)	Cr_2O_3(s)	Cr_2O_3(s)	Cr_2O_3(s)	Cr_2O_3(s)	Cr_2O_3(s)	Cr_2O_3(s)	Cr_2O_3(s)	Cr_2O_3(s)
Ni–S_2–Cl_2	Ni_9S_8(s)	Ni_7S_6(s)/ Ni_9S_8(s)	Ni_7S_6(s)	Ni_9S_8(s)/ Ni_3S_4(s)	Ni_9S_8(s)/ Ni_3S_4(s)	Ni_9S_8(s)	NiS_2(s)	Ni_3S_4(s)/ NiS_2(s)	Ni_3S_4(s)/ NiS_2(s)
Ni–S_2–O_2	Ni_9S_8(s)	Ni_7S_6(s)/ Ni_9S_8(s)	Ni_7S_6(s)	Ni_9S_8(s)/ Ni_3S_4(s)	Ni_9S_8(s)/ Ni_3S_4(s)	Ni_9S_8(s)	NiS_2(s)	Ni_3S_4(s)/ NiS_2(s)	Ni_3S_4(s)/ NiS_2(s)
Ni–Cl_2–O_2	$NiCl_2$(s)	$NiCl_2$(s)	Ni(s)/ $NiCl_2$(s)	$NiCl_2$(s)	$NiCl_2$(s)	Ni(s)/ $NiCl_2$(s)	$NiCl_2$(s)	$NiCl_2$(s)	Ni(s)/ $NiCl_2$(s)

base metals under different conditions and deductive assumptions for their behavior in the alloys will be discussed in the following.

Interactions between HCl and base metal

HCl is very aggressive since it is able to react with the metals to form solid metal chlorides also volatile reaction products (Tables 5 and 6). Thereby, the three base metals show different reactivity with HCl depending on temperature as can be seen from Reactions 1 to 3 in Table 7.

In general, chromium shows the most negative Δ_rG^0 value for the reaction with HCl, followed by iron, and finally by nickel. Thus, chromium will be preferentially attacked by HCl to form chromium chlorides. As soon as all chromium is consumed, iron will react to form its metal chlorides and finally nickel. Since Δ_rG^0 values for the reaction of nickel with HCl are positive at 480°C and 580°C, nickel will mainly remain in its metallic form and will barely react with HCl at these temperatures.

In general, Δ_rG^0 values for the formation of metal chlorides become more negative with decreasing temperature. Thus, the formation of metal chlorides is enhanced at 420°C compared with higher testing temperatures. But in addition to the possible formation of metal chlorides, also their volatile behavior and their vapor pressures have to be considered.

As shown in Table 6, the vapor pressures of several metal chlorides increased with rising temperature and in general, more volatile species are present in the gas phase up to a defined vapor pressure (in Table 6 up to 10^{-15} bar). As previously discussed, it is assumed that mass loss due to evaporation of metal chlorides is significant at pressures ≥ 10^{-4} bar.

As shown in Table 6, the vapor pressures for $FeCl_2$, $Fe(Cl_2)_2$, and $NiCl_2$ are higher than for $CrCl_2$ at all temperatures. Thus, $CrCl_2$, which forms preferentially compared to $FeCl_2$ and $NiCl_2$, will partly remain in the solid corrosion zone. $FeCl_2$, which has the highest vapor pressure, evaporates to a large extent, as soon as it is formed, especially at 580°C. Thus, evaporation of $FeCl_2$ will widely determine the corrosion behavior. $NiCl_2$ contributes only to a small part to the mass loss of the alloys since vapor pressures of $NiCl_2$ are smaller than 10^{-4} bar and since nickel is anyways the last metal to be attacked by HCl. In general, evaporation of metal chlorides is more pronounced at higher temperatures.

Hence, at lower temperatures, the formation of metal chlorides is, on the one hand, preferential due to more negative Δ_rG^0 values, but vapor pressures are much lower and evaporation should only play a subordinate role. Thus, it is expected that formed metal chlorides will remain to a large extent in the corrosion layer.

At 580°C, it can be expected that evaporation of $FeCl_2$ will strongly determine the corrosion behavior if enough $FeCl_2$ can be formed, which depends on the local availability of this alloying element. Alloys with low chromium and high iron content will show a high corrosion rate. In contrast, it seems likely that alloys with a high nickel content and low iron content, are less attacked since nickel will mainly act inert (positive Δ_rG^0).

Interactions between H_2S and base metal

H_2S is able to react with the metals to form several metal sulfides (Table 5). Thereby, the three base metals show different reactivity with H_2S depending on temperature as can be seen from Reactions 4 to 10 in Table 7.

Again, chromium shows the most negative Δ_rG^0 values for the reactions with H_2S, followed by iron and nickel. Thus, chromium will be preferentially attacked by H_2S to form several chromium sulfides. As soon as all chromium is consumed, iron will react to form iron sulfides, whereas the formation of FeS seems more likely than the formation of FeS_2 due to a more negative Δ_rG^0 value (Table 7). In the end, nickel will be attacked by H_2S, whereas the formation of nickel sulfides is possible at all temperatures according to Table 7. In general, Δ_rG^0 values for the formation of metal sulfides become again more negative with increasing temperature.

In addition, the varying amount of H_2S has to be considered, which is not evident from Δ_rG^0 calculations. But as shown in Table 4, the partial pressure of sulfur rises with increasing H_2S content in the gas mixture. Applying these sulfur pressures to the quasi-stability diagrams (Table 8 and Supporting Information Material), it can be indicated that, especially in the high-H_2S atmosphere, the sulfidizing effect is increased.

Interactions between $MeCl_n$ and test gas

Since volatile metal chlorides are formed, which can diffuse outwards, further reactions of those species with the testing gas atmosphere are plausible. In Table 7, several reactions of $MeCl_n$ with gas species revealing negative Δ_rG^0 values are given. Thereby, reactions of metal chlorides with H_2S seem to be the most probable, since reactions with other gas species showed only positive Δ_rG^0 values and Reaction 19 (Table 7) is only possible if H_2O is formed due to the reverse water gas shift reaction (Reaction 16 in Table 7). However, as can be seen, the equilibrium of Reaction 16 is strongly on the educts side and thus, only a very limited amount of H_2O will be formed. The amount of H_2O rises with increasing temperatures and the formation of Cr_2O_3 out of $CrCl_2$ (Reaction 19) is enhanced at 580°C compared with 420°C and 480°C.

Returning to the reactions of metal chlorides with H_2S (Reactions 11–15 in Table 7), Δ_rG^0 values show that $NiCl_2$ will preferentially react with H_2S, followed by $FeCl_2$ and in the end by $CrCl_2$. However, since $NiCl_2$ will only form to a small amount since it is the last metal chloride to be formed and even shows positive Δ_rG^0 values at 480°C and 580°C (Reaction 2 in Table 7), $FeCl_2$ and $CrCl_2$ will contribute to a larger extent to the interactions with H_2S. But since Δ_rG^0 values for the reactions of $CrCl_2$ with H_2S are positive at 420°C and 480°C, formed $CrCl_2$ will either remain in its form or will react with H_2O, if available, according to Reaction 19. Thus, the conversion of $FeCl_2$ with H_2S to FeS seems to be the most feasible one compared with other metal chlorides.

3.2 | Experimental achievements

3.2.1 | Corrosion rates

Even though thermodynamics can be supportive to confirm experimentally achieved statements, it is not able to draw conclusions regarding the severity of a corrosive attack. Therefore, the determination of corrosion rates is helpful, where also differences in the performance of diverse materials can be visualized. In Figures 3–6, the observed corrosion rates of the materials after corrosion experiments at 420°C, 480°C, and 580°C in the low-H_2S, the mid-H_2S, and the high-H_2S mixture are displayed, respectively.

In general, the corrosion rates of the materials increase with increasing temperature and increasing H_2S content, with one exception which was K90941 in the mid-H_2S mixture at 580°C. At lower temperatures, the differences in the corrosion rates of the tested alloys were not significant irrespective of the gas composition. At higher temperatures, these differences increased with rising H_2S amounts. In the low-H_2S mixture, a correlation between the corrosion rate and the nickel content of the alloys was observable at 580°C, whereby the corrosion rates decreased with the increasing nickel content of the alloys. In the high-H_2S mixture, a correlation between the corrosion rates and the chromium content of the alloys was observable at 580°C, whereby materials with higher chromium contents showed the best corrosion resistance. A more detailed analysis of measured corrosion rates and of beneficial alloying elements can be found in previous studies.[18,20,21,25]

Comparing different types of metals, one can say that the ferritic material K90941 showed a poorer corrosion resistance at all conditions than the austenitic materials, with only one unexpected exception, which was the performance of K90941 in the mid-H_2S mixture at 580°C (Figure 8). The corrosion rate of K90941 in the mid-H_2S mixture was even lower than its corrosion rate in the low-H_2S mixture at 580°C. This decrease in the corrosion rate of K90941 will be explained in the following by considering thermodynamic calculations.

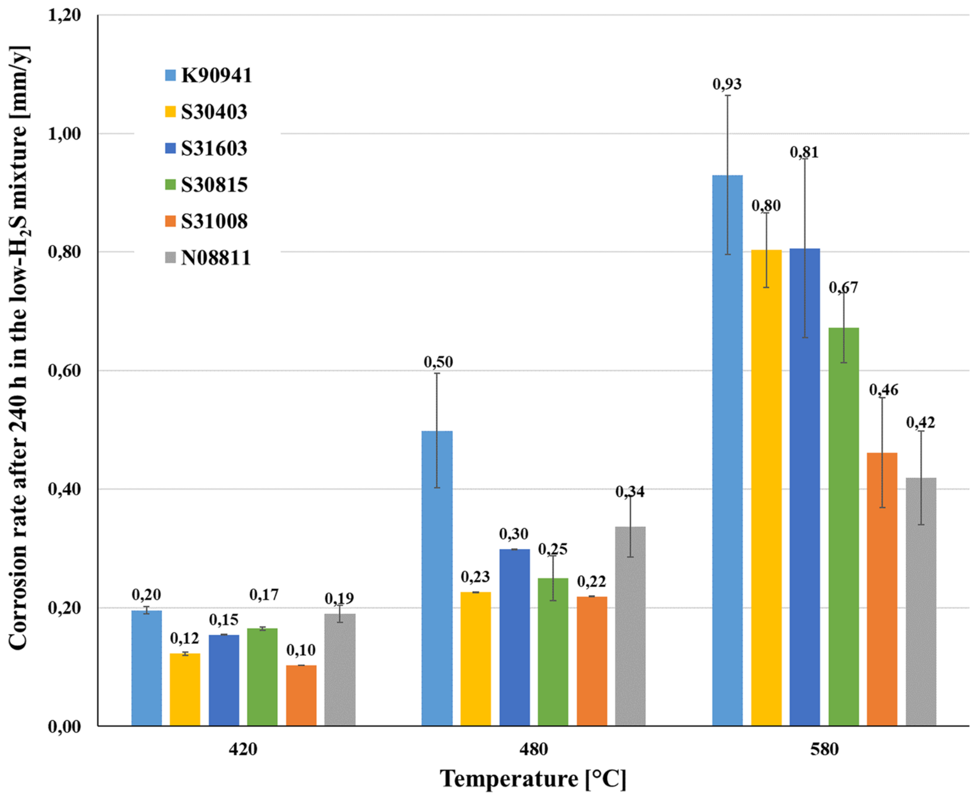

FIGURE 3 Corrosion rates of tested alloys after 240 h experiments in the low-H_2S mixture (0.02 vol% H_2S, 3.8 vol% HCl, 1.9 vol% CO_2, 0.3 vol% CO, 2.8 vol% H_2, bal. N_2) at different temperatures in [mm/y] [Color figure can be viewed at wileyonlinelibrary.com]

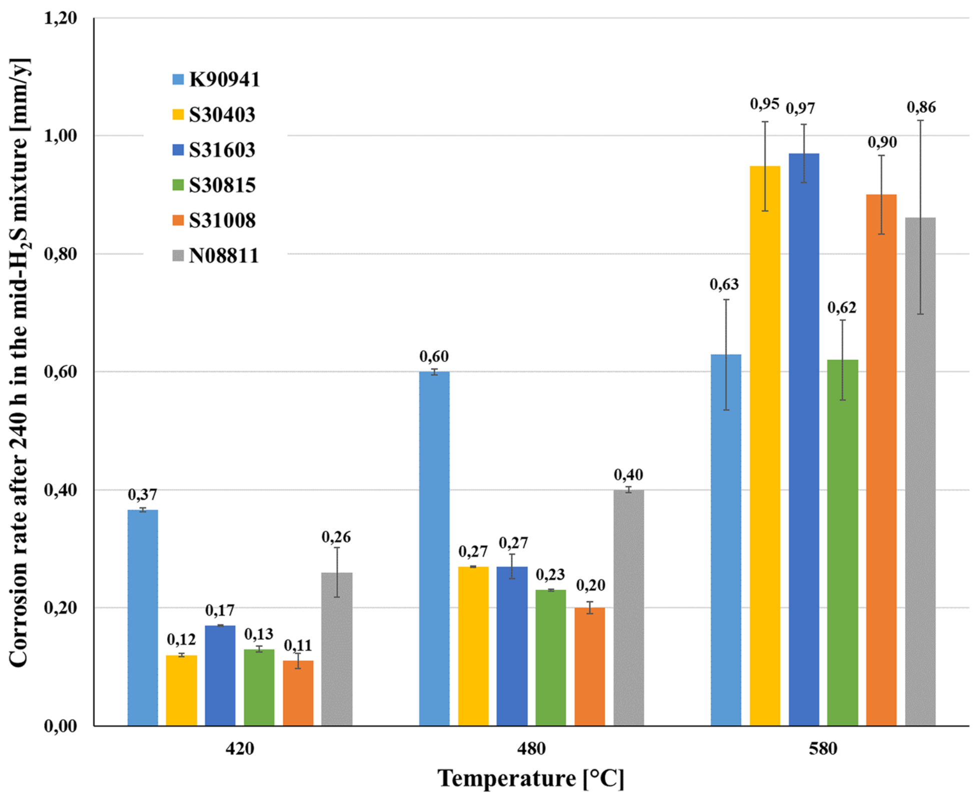

FIGURE 4 Corrosion rates of tested alloys after 240 h experiments in the mid-H_2S mixture (0.2 vol% H_2S, 3.8 vol% HCl, 1.9 vol% CO_2, 0.3 vol% CO, 2.8 vol% H_2, bal. N_2) at different temperatures in [mm/y] [Color figure can be viewed at wileyonlinelibrary.com]

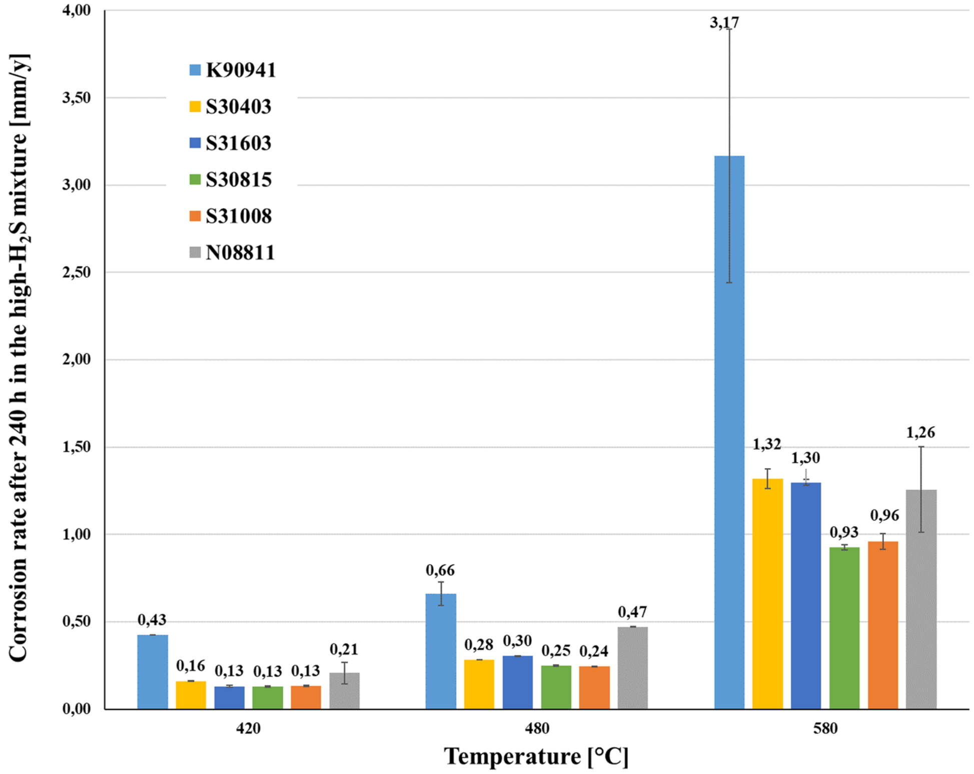

FIGURE 5 Corrosion rates of tested alloys after 240 h experiments in the high-H_2S mixture (2 vol% H_2S, 3.8 vol% HCl, 1.9 vol% CO_2, 0.3 vol% CO, 2.8 vol% H_2, bal. N_2) at different temperatures in [mm/y] [Color figure can be viewed at wileyonlinelibrary.com]

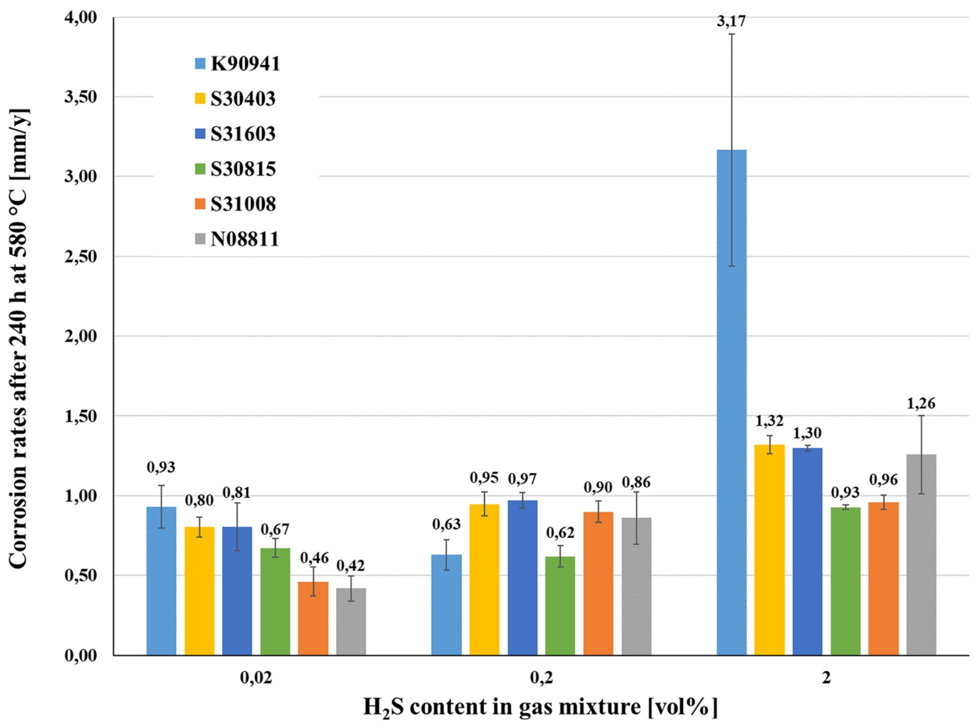

FIGURE 6 Corrosion rates of tested alloys after 240 h experiments at 580°C in different H_2S mixtures (either 0.02 vol%, 0.2 vol%, or 2 vol% H_2S and 3.8 vol% HCl, 1.9 vol% CO_2, 0.3 vol% CO, 2.8 vol% H_2, bal. N_2) in [mm/y] [Color figure can be viewed at wileyonlinelibrary.com]

3.2.2 | Derived corrosion mechanisms

During several studies, experimental know-how in the field of reducing HCl- and H_2S- containing environments was gained (Table 1) and different corrosion mechanisms for diverse alloys under different conditions were developed.[18,20,24,25] These mechanisms are mainly based on practical observations and experience and only less on thermodynamic data. This is due to the complexity of these mixed gas atmospheres, the impact of volatile corrosion products, and the ever-changing conditions within the corrosion layer, which made it hard to predict the actual corrosion behavior.

SEM/EDX mappings, which show the corrosion structures of the ferritic and austenitic alloys, either can be found in previous studies[6,18–22,24,25] or for some selected conditions on representative examples of K90941 and N08811 in Figures 7–14. SEM/EDX mappings of K90941 and N08811 for the remaining conditions can be found in the Supporting Information Materials. Based on the EDX mappings and observations, different corrosion mechanisms for ferritic and austenitic materials could be derived, which are schematically illustrated in Figures 15 and 16, respectively. A detailed explanation of these corrosion structures and the underlying mechanisms can be found in previous studies.[18,20,25]

The corrosion structures differed depending on material, temperature, and gas mixture. In addition, the behavior was strongly determined by the formation of volatile metal chlorides, their possibility to evaporate, and their subsequent reactions with H_2S depending on the amount of H_2S in the gas mixtures. At low temperatures, the materials formed iron sulfide layers on top, whereas in the case of the austenitic materials also nickel was found inside of the iron sulfide layers. Below that layer, a chromium sulfide layer could be detected. The same corrosion structures could be observed at high temperatures in the mid-H_2S and high-H_2S mixture, whereas in the case of the austenitic materials almost no nickel was found in the iron sulfide layer. In the low-H_2S mixture at high temperatures, the corrosion structures revealed a chromium sulfide layer on top. Iron was only found as precipitated $FeCl_2$ in the colder parts of the test equipment. The reasons for the differences of the corrosion structures

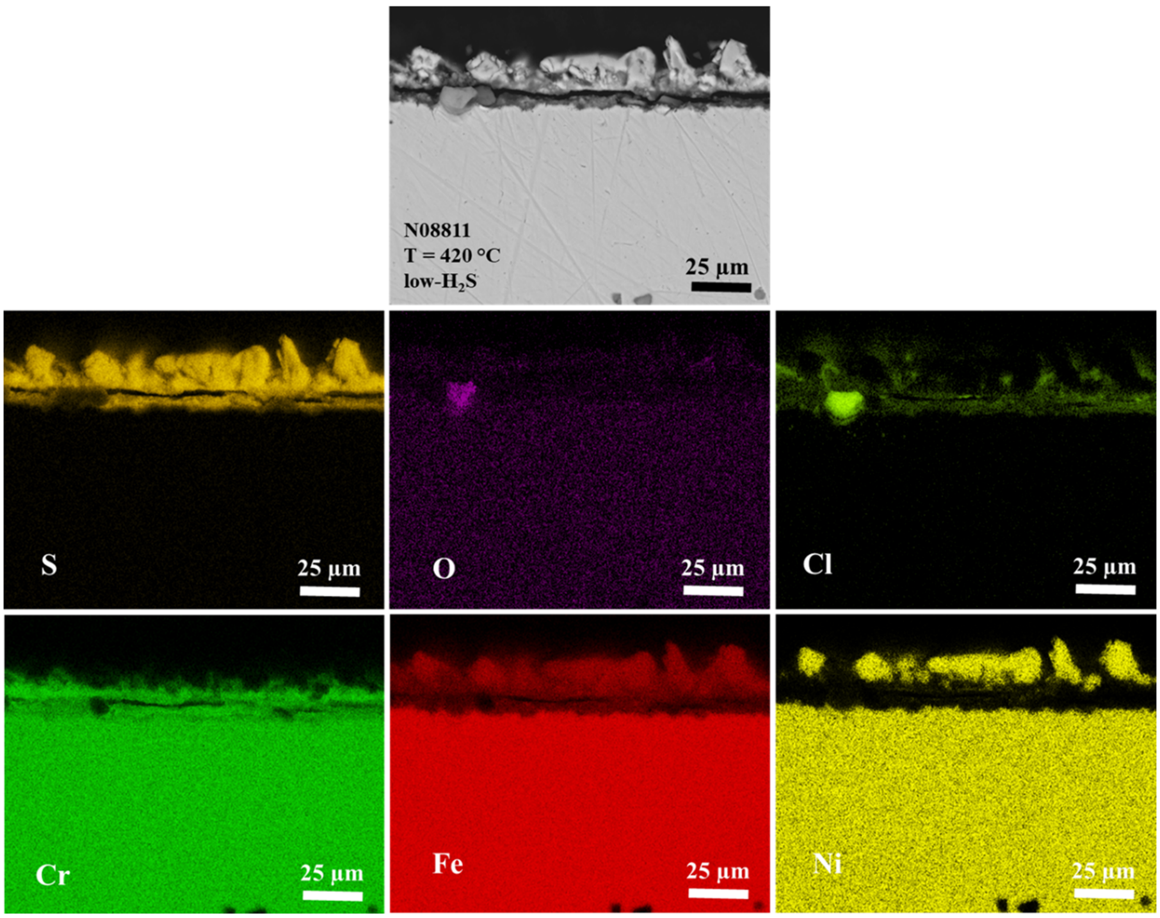

FIGURE 7 N08811 after 240 h, low-H_2S mixture, 420°C. SEM and EDX element mapping of the cross-section. [Color figure can be viewed at wileyonlinelibrary.com]

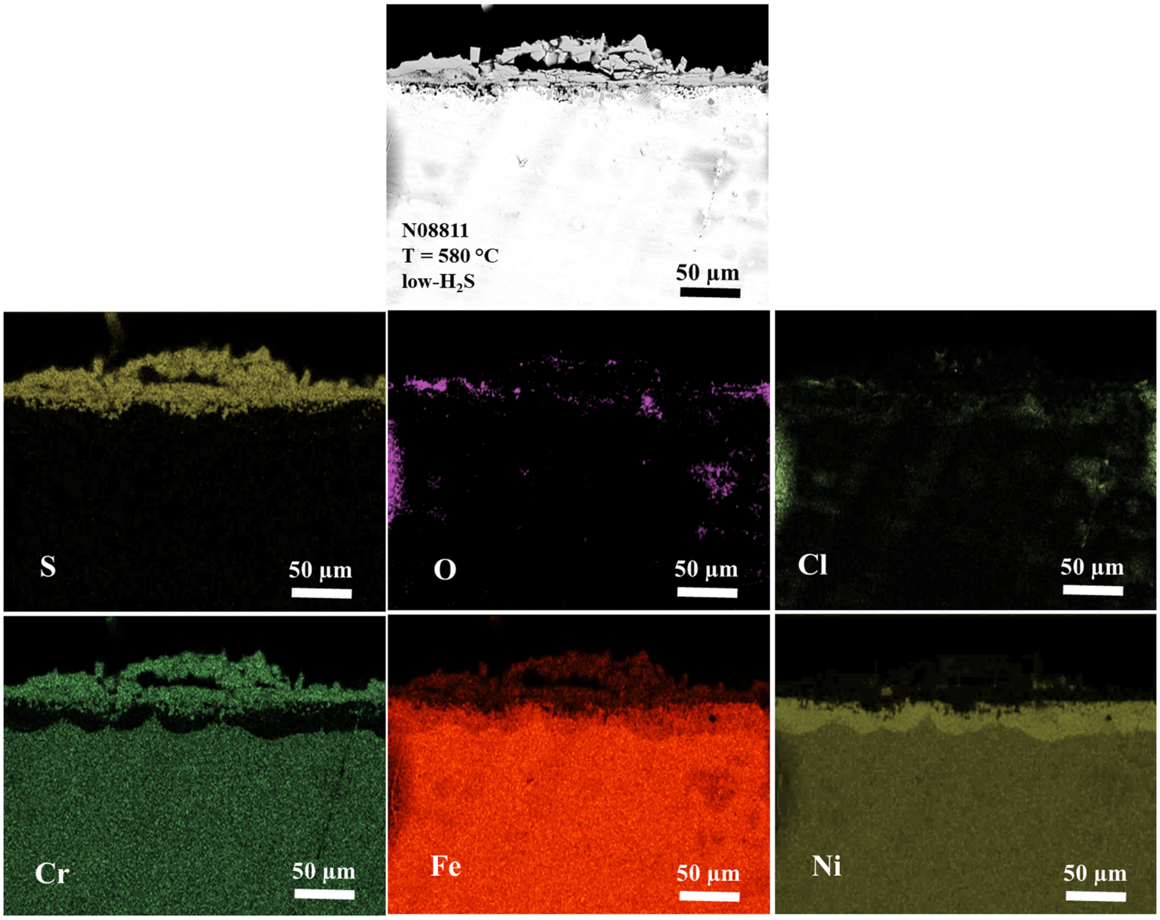

FIGURE 8 N08811 after 240 h, low-H_2S mixture, 580°C. SEM and EDX element mapping of the cross-section. [Color figure can be viewed at wileyonlinelibrary.com]

and the derived corrosion mechanisms will be explained in the following by means of thermodynamics.

3.3 | Correlation of thermodynamic data and experimental achievements

Thermodynamic data will be discussed on basis of the determined corrosion rates (Figures 3–6) and previously derived and expanded corrosion mechanisms for ferritic and austenitic materials, which are schematically shown in Figures 15 and 16, respectively.[18,20,25] The correlation between the thermodynamically predicted corrosion products and the experimental received results is discussed in the following.

3.3.1 | Formation of volatile metal chlorides

HCl is very aggressive since it is able to form volatile metal chlorides, whereas the severity of their evaporation depends on temperature. The vapor pressures of individual corrosion products increase with rising temperature (Table 6). Thus, at higher temperatures more volatile products are formed, which affect the corrosion behavior. Thereby, a partial pressure above 10^{-4} bar is assumed as critical for volatile corrosion products. Thus, especially the formation of $FeCl_2$ at 580°C damages the materials.

This damaging effect of volatile species could be verified in the low-H_2S mixture on basis of precipitated $FeCl_2$ at colder parts of the laboratory test equipment. $FeCl_2$ that was formed on the samples due to the reaction of Fe + HCl was carried away with the gas flow and recrystallized at colder sites. In the mid-H_2S mixture, this effect was only partially observed, whereas in the high-H_2S mixture it was not detected anymore.

In general, the amount of detected metal chlorides varied depending on temperature and gas mixture, which is visualized in Table 9. With the rising temperature, the amount of $FeCl_2$ also increased, especially in the low- and mid-H_2S mixture, which is in accordance with the increasing vapor pressures in Table 6. However, the amount in the mid-H_2S mixture was still less at the same temperature compared with the low-H_2S mixture.

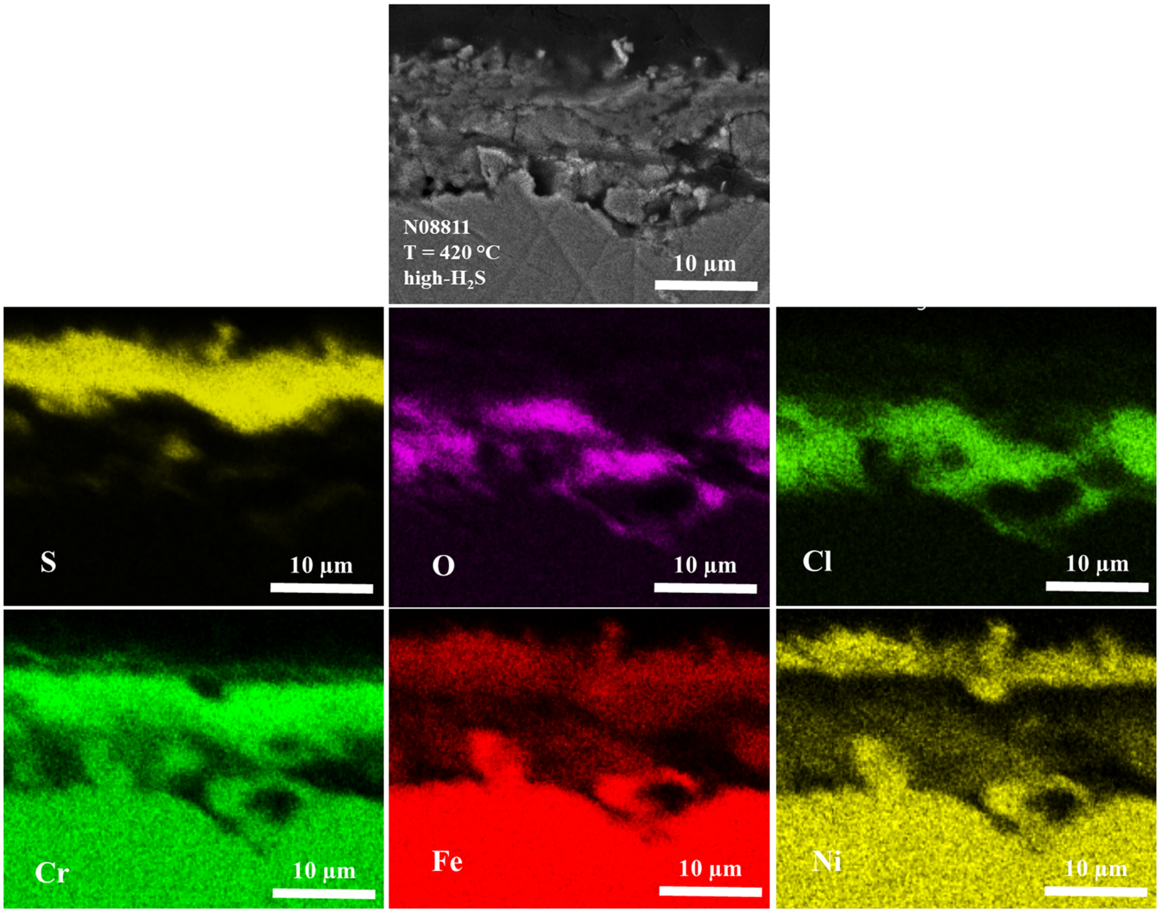

FIGURE 9 N08811 after 240 h, high-H_2S mixture, 420°C. SEM and EDX element mapping of the cross-section. [Color figure can be viewed at wileyonlinelibrary.com]

In addition, the amount of precipitated $FeCl_2$ also varied depending on the material, whereby materials with higher iron content, like K90941, formed more $FeCl_2$ than materials with smaller iron content, like N08811. The enhanced evaporation of $FeCl_2$ of materials with higher iron content could also be reflected in the higher corrosion rates. Thus, K90941 showed the highest corrosion rate at 580°C in the low-H_2S mixture due to the strong evaporation of $FeCl_2$ compared with other materials with less iron (Figure 3).

Several authors reported the significant formation of volatile corrosion products at even much lower partial pressures than 10^{-4} bar, and that the risk of evaporating corrosion species should not be underrated.[37] This was also verified during our studies as the vapor pressure of $FeCl_2$ at 420°C was calculated to be 10^{-6} bar, but it still precipitated at colder parts of the test equipment in the low-H_2S mixture. In addition, the vapor pressure of $CrCl_3$ at 580°C was calculated to be 10^{-10} bar. Despite the low vapor pressure, it was detected by XRD analysis after experiments in the low-H_2S mixture at 580°C (Figure 17). Besides $FeCl_2$ and $CrCl_3$, XRD identified also $FeCl_2(H_2O)_2$, whereby hydration of $FeCl_2$ happened due to the hygroscopic behavior of $FeCl_2$ and the reaction with water from the environment and not due to the corrosion process itself.

In the high-H_2S mixture, no precipitated $FeCl_2$ could be detected, not even at high temperatures, although thermodynamic predictions revealed the formation of metal chlorides (Table 5) and also vapor pressures were the same as for the low-H_2S and mid-H_2S mixture (Table 6). This behavior will be discussed later on.

Another indication of the attack of HCl, besides the precipitated metal chlorides, can be found in the Cl-EDX mappings of the materials (representative examples of K90941 and N08811 can be found in Figures 7–14 and in the Supporting Information Material). In Cl-EDX mappings of several materials, a certain amount of chlorine could be detected under all conditions, even in the high-H_2S mixture. Thus, Reactions 1 to 3 (Table 7) still take place in the high-H_2S mixture.

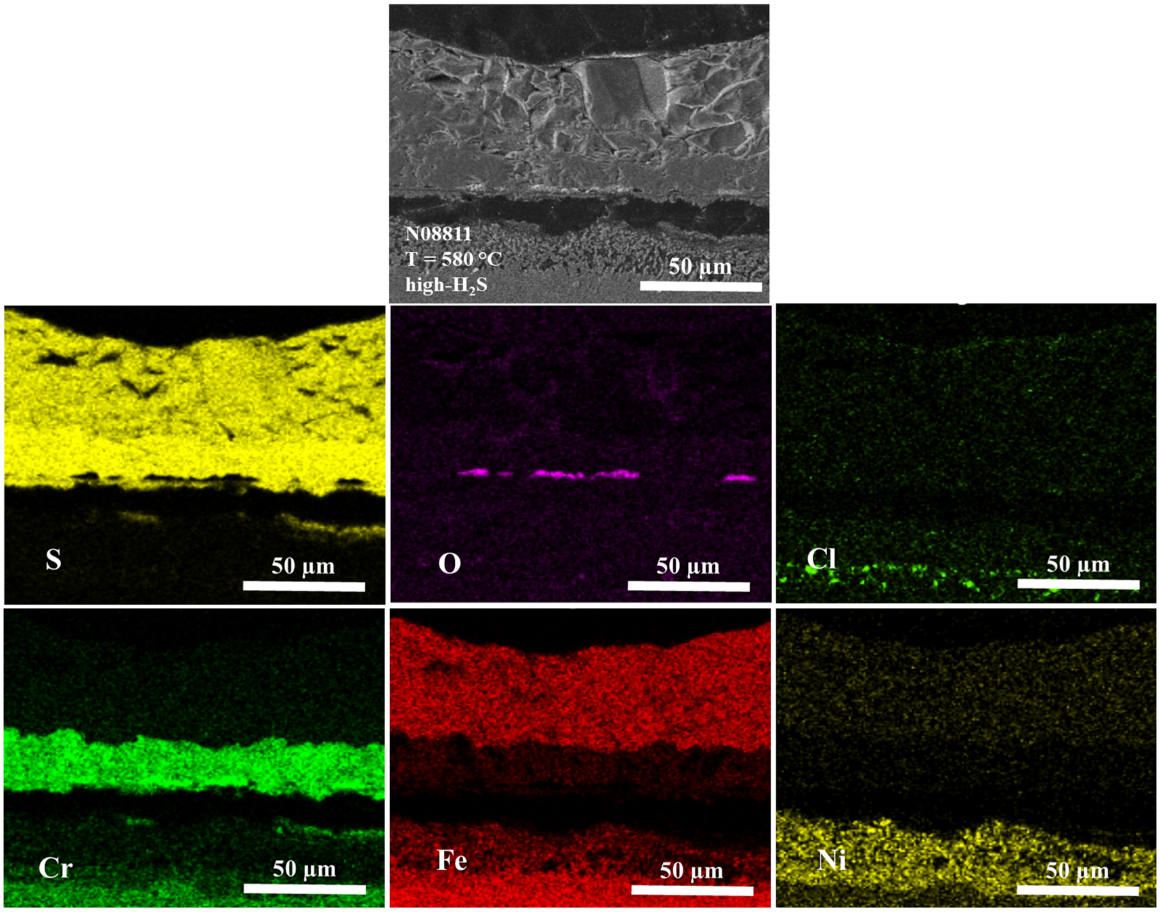

FIGURE 10 N08811 after 240 h, high-H_2S mixture, 580°C. SEM and EDX element mapping of the cross-section. [Color figure can be viewed at wileyonlinelibrary.com]

However, besides metal chlorides also several metal sulfides were detected during the experiments. And even though the HCl content was identical in all gas mixtures (3.8 vol%), the same materials showed different behaviors in the three mixtures, also at the same temperature. This could be verified by altering corrosion rates (Figures 3–6). Thus, the varying amount of H_2S and its interaction with HCl and volatile species has to be considered.

3.3.2 | Formation of metal sulfides

As thermodynamically predicted, the formation of several metal sulfides could be observed during experiments. Thereby, the severity of sulfide formation varied depending on material, temperature, and gas mixture. In general, the ferritic material was stronger attacked than austenitic materials and the sulfide scales increased with rising temperature and rising H_2S content in the gas mixture, which could be reflected in the corrosion rates (Figures 3–6). Thus, in the high-H_2S mixture, the strongest tendency to form metal sulfides was observed, as also indicated by quasi-stability diagrams (Table 8).

Besides the thickness of sulfide scales, also the structure of the scales varied as schematically shown in Figures 15 and 16. For example, in the low-H_2S mixture at high temperatures, no iron sulfide was detected on the surface, as was found in all other conditions, even though it was thermodynamically predicted (Table 5). But instead, chromium sulfide formed on top of the corrosion products.

As shown in Table 7 and Figure 1, chromium is the first base metal that reacts with H_2S. Thus, the formation of chromium sulfide would not be surprising. However, in the mid-H_2S and high-H_2S mixture also iron sulfides could be detected on the surface at 580°C. The reason for the altering corrosion structure in the mid-H_2S and high-H_2S mixture can be found in the higher amount of available H_2S in the gas phase. But besides the higher amount of H_2S, also outwards diffusing metal chlorides that have formed, have to be considered. These interactions of the base metals and metal chlorides with HCl and a varying amount of H_2S and their possible prediction with thermodynamics will be discussed in the following.

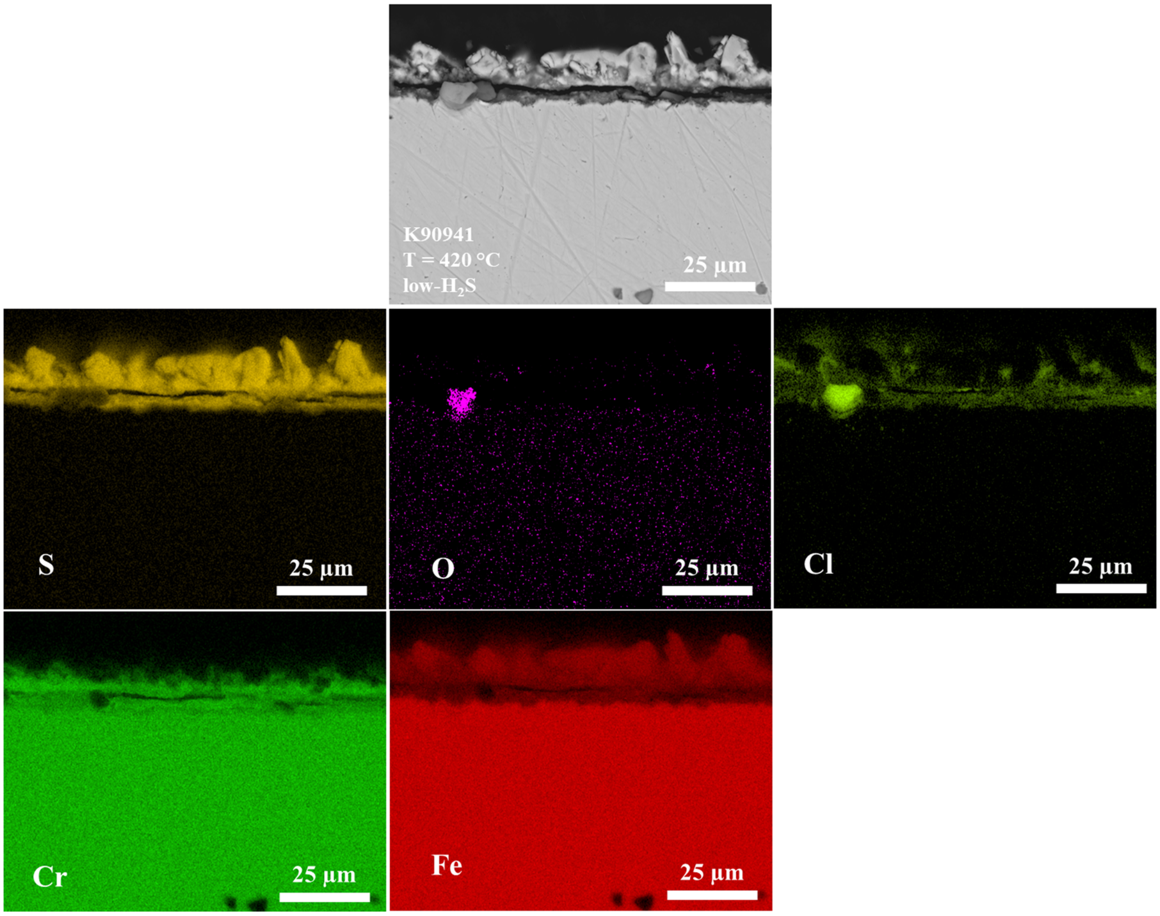

FIGURE 11 K90941 after 240 h, low-H_2S mixture, 420°C. SEM and EDX element mapping of the cross-section. [Color figure can be viewed at wileyonlinelibrary.com]

3.3.3 | Interaction between gas mixture, volatile species, and alloys

Comparing the corrosion rates (Figures 3–6), as well as the corrosion mechanisms (Figures 15 and 16), one can see that several differences were observed. Furthermore, various beneficial alloying elements could be allocated under different conditions as mentioned before. For assessment and explanation of these corrosion rates and corrosion mechanisms, thermodynamics can be a very useful tool.

Therefore, the derived corrosion mechanisms of ferritic and austenitic materials can roughly be divided into the behavior at lower testing temperatures (420°C and 480°C) and into the behavior at higher testing temperatures (580°C). For sake of simplicity and since the observed corrosion behaviors of the materials are similar at 420°C and 480°C, these two temperatures are considered together, even though some deviations in thermodynamic data occur, which is discussed afterward. In addition to temperatures, it has to be differentiated between the supply of H_2S in the gas phase thus, the behavior in the low-, the mid-and the high-H_2S mixture.

Behavior of materials in the low-H_2S mixture at low temperatures

The most reactive base metal is chromium, whereas chromium will primarily react with HCl and H_2S to form metal chlorides and metal sulfides, respectively, thereby establishing the base of the corrosion zone. After chromium, iron will be attacked followed by nickel.

At lower temperatures, the formation of metal chlorides will more easily take place than at higher temperatures due to more negative Δ_rG^0 values. In addition, contrary to higher temperatures, the formation of $NiCl_2$ is thermodynamically predicted, which has to be considered for austenitic materials.

However, the volatility of the formed metal chlorides is not as pronounced as at high temperatures. Thus, they will remain a big part of the corrosion layer. Due to their long residence time in the corrosion zone, the conversion of metal chlorides to metal sulfides by reaction with H_2S is possible, even though only a small amount of H_2S is present in the gas phase.

Since vapor pressures of $FeCl_2$ and $NiCl_2$ are slightly higher than those of $CrCl_2$, these two metal chlorides can

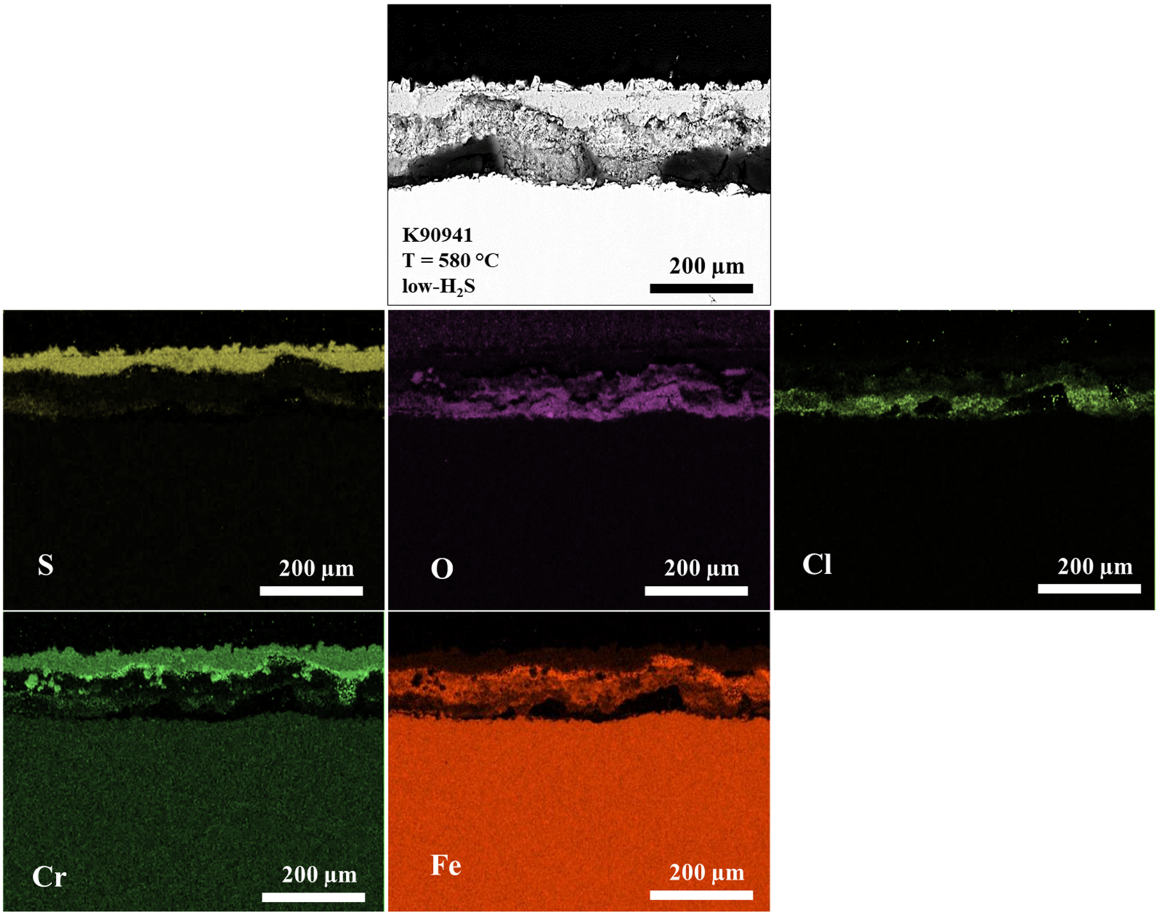

FIGURE 12 K90941 after 240 h, low-H_2S mixture, 580°C. SEM and EDX element mapping of the cross-section. [Color figure can be viewed at wileyonlinelibrary.com]

diffuse outwards until they react with H_2S. Therefore, an iron-nickel-sulfide layer has formed on top of the austenitic materials. Since the ferritic material does not contain nickel, only an iron sulfide layer could be found on the surface of the material.

Due to the low vapor pressures of formed metal chlorides, also no big deviations between the ferritic material and the austenitic materials can be observed. An explanation of the mechanism in the low-H_2S mixture at low temperatures based on experimental considerations can be found elsewhere.[20]

Behavior of materials in the low-H_2S mixture at high temperatures

At high temperatures, the corrosion rates of the materials decreased with increasing nickel and decreasing iron content (Figure 3). From a thermodynamic point of view, it seemed likely that alloys with a high nickel content and low iron content are less attacked since nickel will mainly act inert (positive Δ_rG^0). This could be verified during experiments since an accumulation of nickel in the border zone of the metals could be observed in the SEM/EDX mappings of austenitic materials. This is also in accordance with Ni–Cl_2–O_2 quasi-stability diagrams (Table 8) since they revealed that affecting partial pressures of chlorine and sulfur of the low-H_2S mixture are at the border area of metallic nickel and $NiCl_2$. In addition, nickel would be the last metal to react with H_2S, after chromium and iron, and since only a small amount of H_2S is available other reactions are preferred.

The rise of corrosion rates with increasing iron content can therefore be explained by the unhindered evaporation of $FeCl_2$ and also no further reaction with H_2S due to a too small amount of this gas species in the mixture. At 580°C, evaporation of $FeCl_2$ will strongly determine the corrosion behavior, if enough $FeCl_2$ can be formed, which depends on the local availability of this alloying element, which was confirmed by the high corrosion rate of K90941.

Thus, the high vapor pressure of metal chlorides at high temperatures (Table 6) and the small partial pressure of sulfur in the low-H_2S mixture (Table 4), as well as favored reactions of chromium with H_2S due to more negative Δ_rG^0 values (Table 7), can explain why in case of the low-H_2S

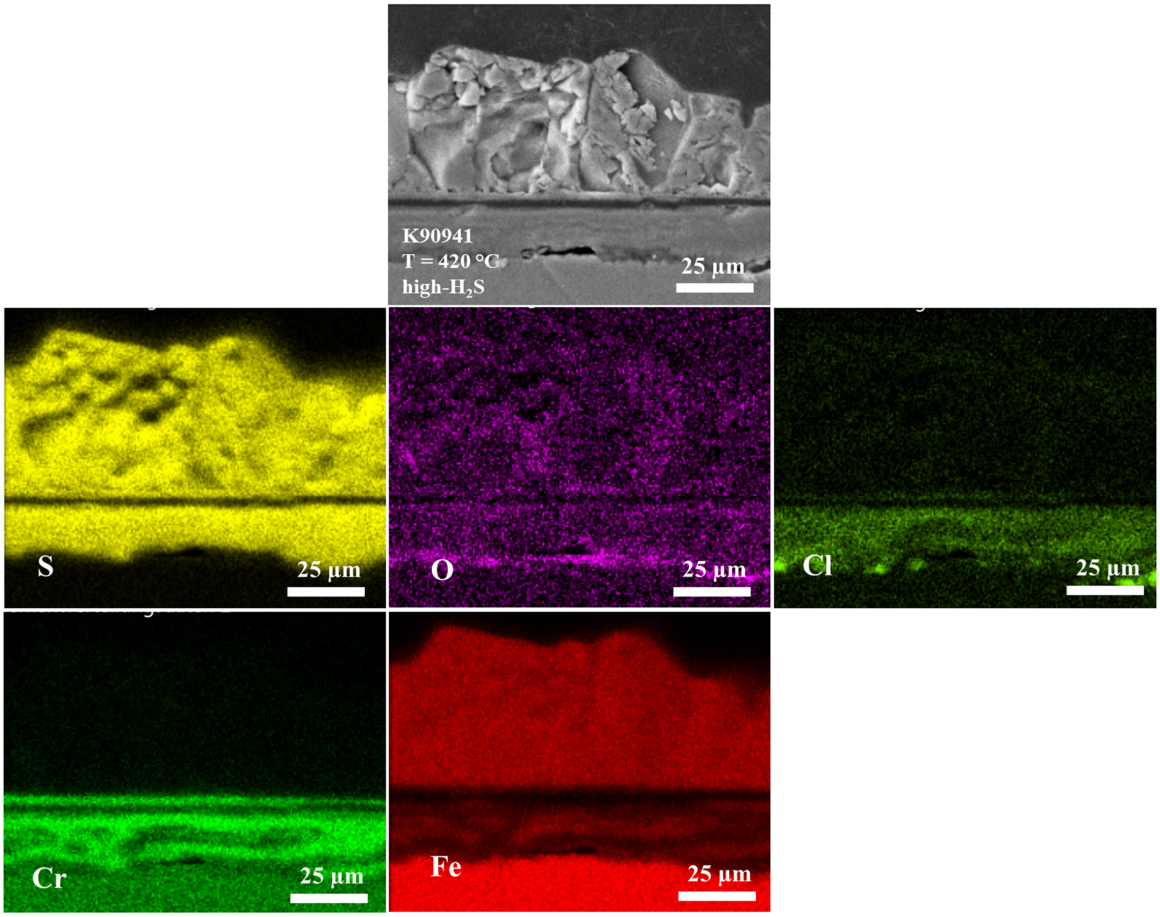

FIGURE 13 K90941 after 240 h, high-H_2S mixture, 420°C. SEM and EDX element mapping of the cross-section. [Color figure can be viewed at wileyonlinelibrary.com]

mixture at high temperatures, chromium sulfide had formed on top. An explanation of the mechanism in the low-H_2S mixture at high temperatures based on experimental considerations can be found elsewhere.[18]

Behavior of materials in the mid-H_2S mixture at low temperatures

The same principles as for the low-H_2S mixture at low temperatures are applicable for the mid-H_2S mixture at low temperatures. The only difference is that the sulfide formation proceeds to a larger extent due to a higher amount of H_2S in the gas phase, but otherwise, corrosion structures, corrosion rates, and also predicted corrosion products were similar.

Behavior of materials in the mid-H_2S mixture at high temperatures

In the mid-H_2S mixture at high temperatures, the corrosion behavior of the materials is different compared with the low-H_2S mixture. While in the low-H_2S mixture chromium sulfide was detected on top of the corrosion products, in the mid-H_2S mixture iron sulfide was observed. The reason for the altered corrosion structures can be found in the higher H_2S content of the mid-H_2S mixture.

As for the low-H_2S mixture, Δ_rG^0 values and vapor pressures of volatile metal chlorides are the same for all atmospheres. Thus, the formation of $CrCl_2$ and $FeCl_2$ still takes place at 580°C. Again, $CrCl_2$ mainly remains in the corrosion zone, where it further reacts to form other corrosion products, whereas $FeCl_2$ evaporates due to its high vapor pressure. However, since the reaction of $FeCl_2$ with H_2S revealed a strongly negative Δ_rG^0 value at 580°C (Reaction 11 in Table 7) and since enough H_2S is available in the gas phase, a certain amount of the outwards diffusing $FeCl_2$ is converted to FeS, which can be detected as corrosion layer on the surface. The rest of the outwards diffusing $FeCl_2$, which does not find H_2S to react, still evaporates but compared with the low-H_2S mixture this amount of $FeCl_2$ that is able to evaporate without conversion to FeS is less in the mid-H_2S mixture. This could be verified by a smaller amount of precipitated $FeCl_2$ (Table 9).

Comparing the corrosion rates of austenitic materials with the ferritic material K90941 in the mid-H_2S mixture

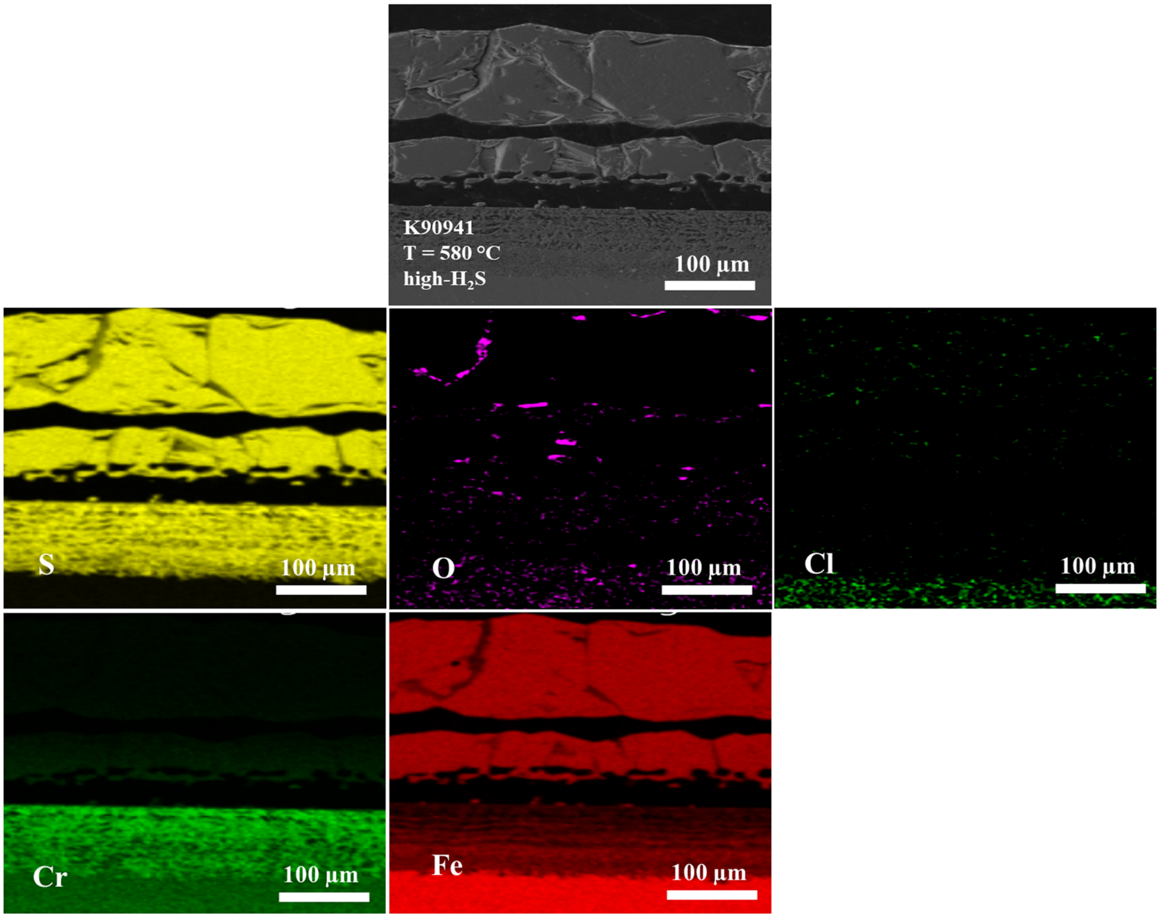

FIGURE 14 K90941 after 240 h, high-H_2S mixture, 580°C. SEM and EDX element mapping of the cross-section. [Color figure can be viewed at wileyonlinelibrary.com]

at 580°C; Figures 4–6), it can be seen that K90941 performed better than the austenitic materials. This was unexpected since K90941 showed during all other test conditions a poorer corrosion resistance compared with the austenitic materials. The improved behavior of K90941 in the mid-H_2S mixture at 580°C compared with the low-H_2S mixture and to other materials can be explained as follows:

As identified, in the low-H_2S mixture formed metal chlorides, especially $FeCl_2$, can easily evaporate at 580°C due to their high vapor pressure. In addition, no further reaction of $FeCl_2$ with H_2S to FeS will occur due to a too small amount of H_2S in the gas phase and favored reactions of this gas species with chromium (Table 7). Since K90941 contains a high amount of iron, the mass loss is strongly attributed to the continuous evaporation of $FeCl_2$. Austenitic materials contain less iron and subsequently volatilization of metal chlorides is a smaller issue. Additionally, K90941 has the smallest amount of chromium. Thus, the chromium sulfide and chromium oxide layers that form on K90941 represent diffusion barriers that are not as protective and uniform as those formed on austenitic materials with higher chromium content. In addition, austenitic materials contain nickel, which rarely reacts to these conditions, thus a part of these metals is inert. Since the corrosion behavior in the low-H_2S mixture is widely dominated by chlorination processes, the lower corrosion resistance of K90941 compared with the austenitic materials can be explained.

However, in the mid-H_2S mixture things change and K90941 performs suddenly best. The reason for this behavior might be found in the quasi-stability diagram of the system Fe–Cl_2–S_2 at 580°C (Figure 2). As illustrated by the blue circle, the partial pressures of chlorine and sulfur are right at the border between the stability of $FeCl_2$ and FeS. It seems likely that competing processes between the formation of $FeCl_2$ and FeS occur, which slow down the corrosive attack. H_2S and HCl might compete simultaneously for the predominance of iron and depending on local partial pressures of sulfur and chlorine, which can locally change due to various reactions, either H_2S or HCl will finally react with iron. Due to the iron-dominated character of K90941, an approximation to thermodynamic calculations of pure

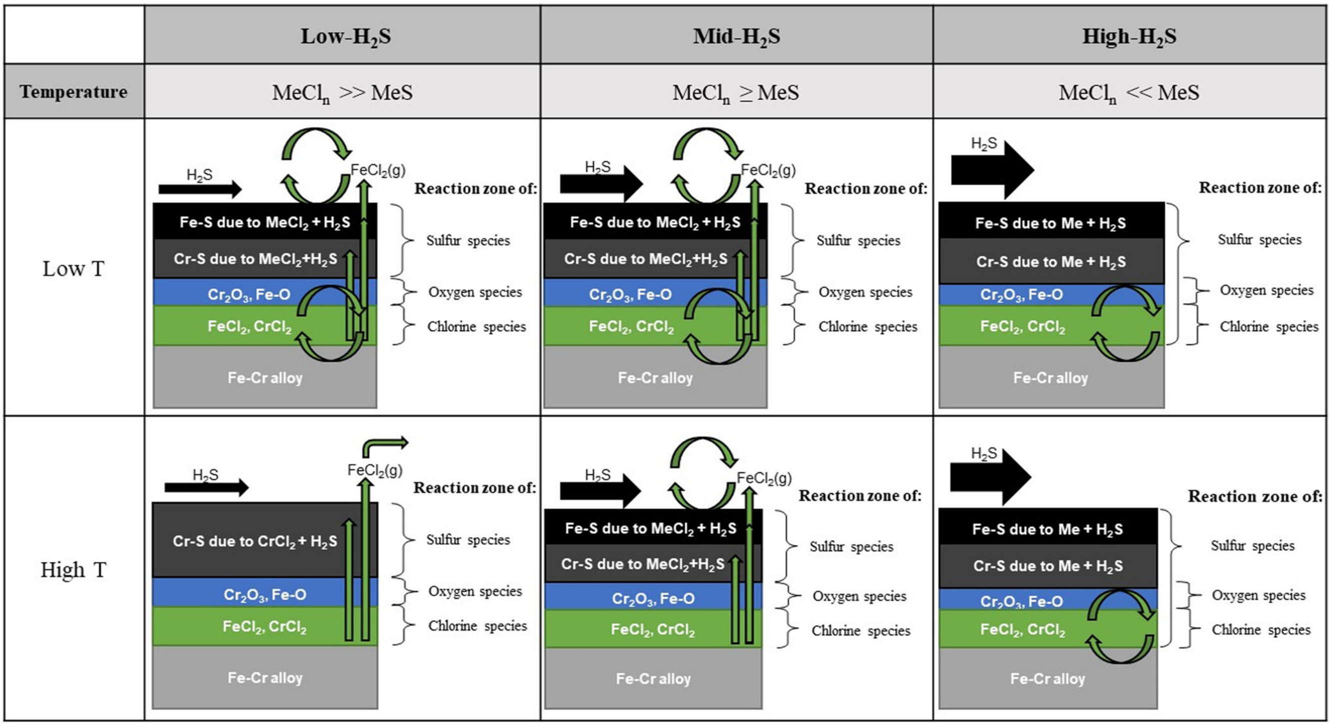

FIGURE 15 Corrosion mechanisms of ferritic K90941 in different H_2S-mixtures at different temperatures (derived and evolved from[18,20,25]). Low T indicating temperatures of 420°C and 480°C, high T indicating a temperature of 580°C. [Color figure can be viewed at wileyonlinelibrary.com]

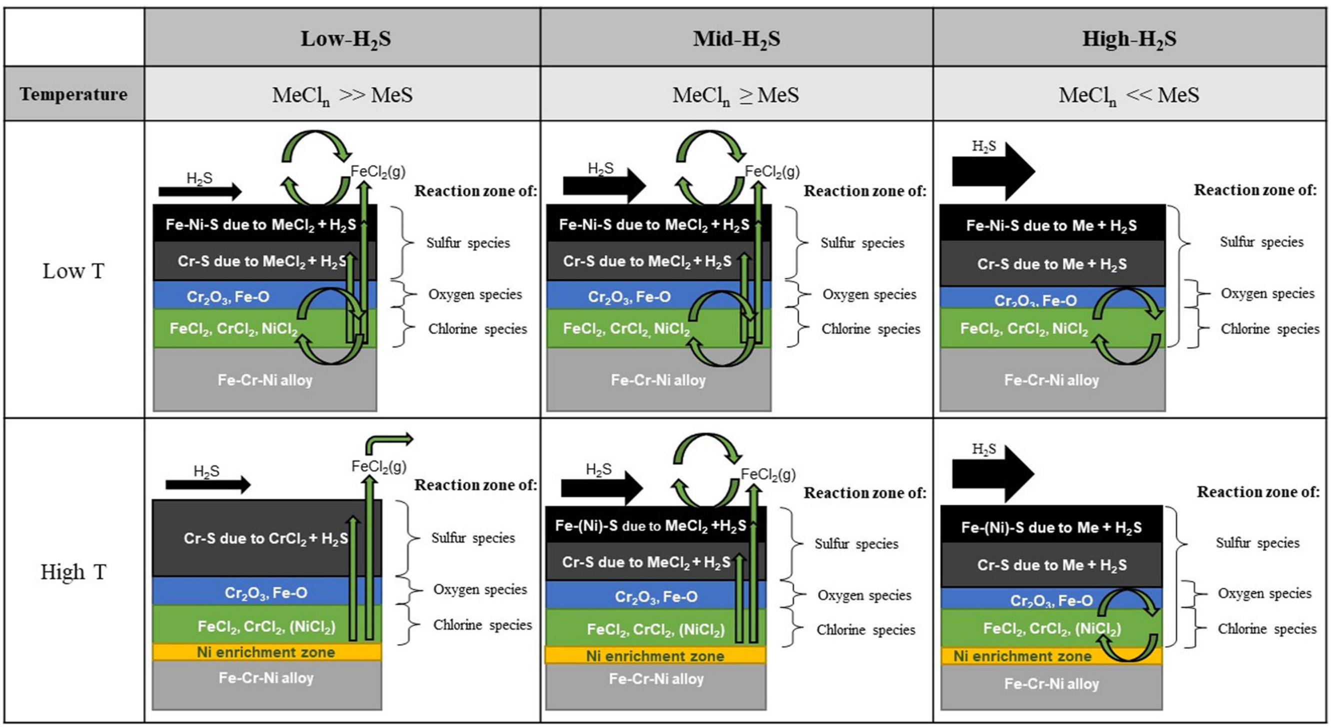

FIGURE 16 Corrosion mechanisms of austenitic materials in different H_2S-mixtures at different temperatures (derived and evolved from[18,20,25]). Low T indicating temperatures of 420°C and 480°C, high T indicating a temperature of 580°C. [Color figure can be viewed at wileyonlinelibrary.com]

iron seems to be suitable. With this, it can be seen that under certain partial pressure ratios, corrosion inhibition of ferritic materials can happen due to competing corrosion processes. Since austenitic materials contain a more balanced ratio of alloying elements, which determine other sulfide formation processes, these materials show a higher corrosion rate in the mid-H_2S mixture at 580°C.

Behavior of materials in the high-H_2S mixture at low temperatures

According to thermodynamic equilibrium calculations and quasi-stability diagrams, a stronger tendency of sulfide formation can be expected in the high-H_2S mixture. This could be verified among others with the nondetectable amount of precipitated $FeCl_2$. As for the low-H_2S and the mid-H_2S mixture, the formation of several metal chlorides is thermodynamically still possible. However, due to the oversupply of H_2S in the gas phase, this gas species can penetrate the corrosion layer up to the deepest regions, so that outward diffusing metal chlorides do not get far enough to evaporate before they are converted. Thereby, the reaction $MeCl_2 + H_2S \rightarrow FeS + 2\ HCl$ will take place, whereby more HCl gas is generated. This released HCl accumulates in the deepest regions of the corrosion zone, where it can again react with the base metal to form metal chlorides, thereby generating an HCl circle, as schematically shown in Figures 15 and 16. An explanation of the mechanism in the high-H_2S mixture at low temperatures based on experimental considerations can be found elsewhere.[25]

TABLE 9 Detected amount of $FeCl_2$ at colder parts of laboratory test equipment

	Qualitative amount of $FeCl_2$ condensing outside of tube furnace		
Temperature	**Low-H_2S**	**Mid-H_2S**	**High-H_2S**
Low T	Medium	Little	No
High T	High	Medium	No

Behavior of materials in the high-H_2S mixture at high temperatures

From a thermodynamic point of view, a stronger tendency of sulfide formation can be expected in the high-H_2S mixture compared with the low-H_2S and the mid-H_2S mixture. For example, quasi-stability diagrams of the system $Fe–S_2–Cl_2$ and $Cr–S_2–Cl_2$ (Table 8) revealed that the corrosion behavior of the high-H_2S mixture is strongly dominated by sulfide formation processes. At 580°C, also the reaction of chromium with H_2S is favored toward the reaction with HCl, as illustrated in Figure 1.

However, the formation of $CrCl_2$ and $FeCl_2$ is thermodynamically still predicted (Reactions 1 and 2 in Table 7), whereas the formation of $NiCl_2$ will only contribute to a very small amount due to positive Δ_rG^0 values. Since also the reaction of nickel with H_2S would be the last to take place due to the less negative Δ_rG^0 value (Table 7), nickel partly remains metallic. This could be verified by an accumulation of nickel in the border zone of the metals in several SEM/EDX mappings of austenitic materials.

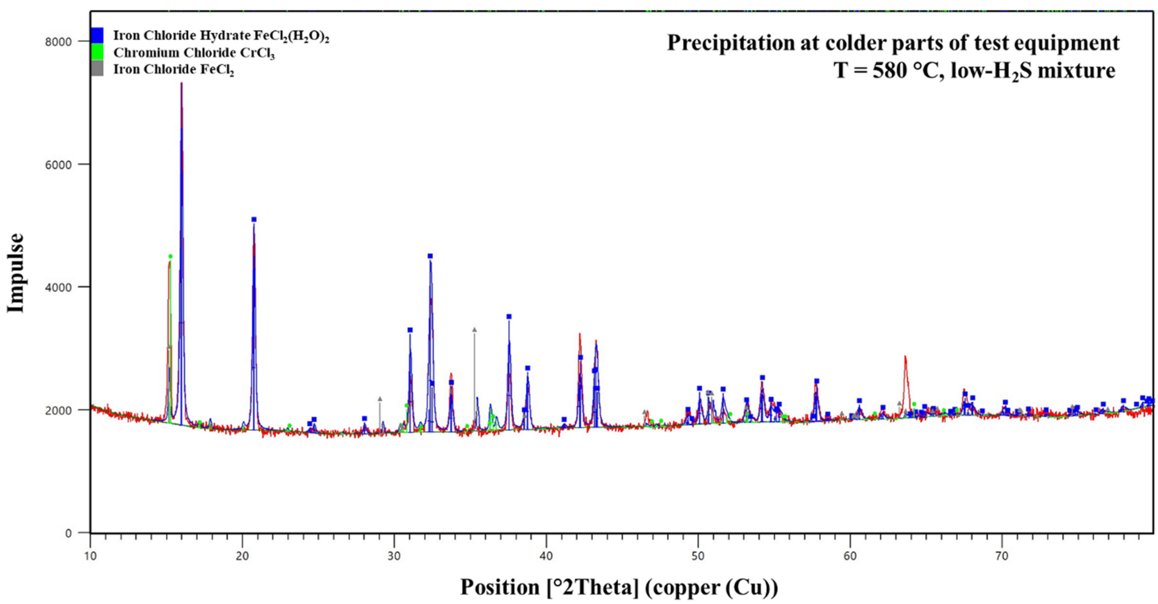

FIGURE 17 X-ray diffraction pattern of precipitated $FeCl_2$ and $CrCl_3$ at 580°C in the low-H_2S mixture [Color figure can be viewed at wileyonlinelibrary.com]

Same as for low temperatures, the stronger tendency to form sulfides could be verified, among others, with the nondetectable amount of precipitated $FeCl_2$ (Table 9). While in the low-H_2S mixture too little H_2S is available, which can convert $FeCl_2$ to FeS, things are different in the high-H_2S mixture. Due to an oversupply of H_2S, all formed $FeCl_2$ can react with H_2S to FeS. Additionally, due to the high sulfur partial pressure also sulfidation of the base metal itself can take place.

As already identified for lower temperatures, the reaction of $MeCl_2 + H_2S$ will release HCl, which remains in the deepest regions of the corrosion zone, where it can further react with the base metal to form metal chlorides generating an HCl circle, as schematically shown in Figures 15 and 16. Due to this circular process, it is plausible that the partial pressure of chlorine is higher than in regions where metal chlorides can evaporate.

In the high-H_2S mixture, chromium was identified to be beneficial by slowing down the corrosive attack at 580°C (Figure 5), among others due to the formation of $FeCr_2S_4$.[21,25] The favored reactions of chromium with the gas phase as indicated in Table 7 and the less pronounced behavior of metal chlorides as indicated by quasi-stability diagrams (Table 8), might explain this behavior. The high corrosion rates of K90941 can be attributed to the nonprotective effect of iron sulfide compared with that of chromium sulfide, whereby the corrosion process can proceed faster. Since austenitic alloys contain more chromium than K90941, subsequently thicker and denser chromium sulfide layers can form, explaining the better resistance of these materials. An explanation of the mechanism in the high-H_2S mixture at high temperatures based on experimental considerations can be found elsewhere.[25]

3.3.4 | Deviations between thermodynamic calculations and experimental results

Some deviations between thermodynamically predicted products and experimental results were observed during the thermodynamic analysis. For example, thermodynamic equilibrium calculations revealed the formation of Cr_2N (Table 5). However, no Cr_2N could be detected during the experiments. The reason for the prediction of Cr_2N can be explained by the definition of parameters used for thermodynamic equilibrium calculations. For the calculations, an excess amount of chromium (1000 mole) was chosen, as well as a high amount of nitrogen to balance the gas mixture. From a thermodynamic point of view, it is therefore plausible that the formation of Cr_2N will take place if a surplus of both components is available and if the achievement of thermodynamic equilibrium is assumed.

Another example is the reaction of nickel with HCl to form $NiCl_2$. According to Reaction 2 in Table 7, the formation of $NiCl_2$ should hardly take place at 480°C since positive $\Delta_r G^0$ values were calculated. However, during a previous study, it was identified that the formation of $NiCl_2$ still occurs and contributes to the corrosion mechanism at low temperatures.[20]

In general, chemical equilibrium can be calculated if a system is defined in terms of temperature, pressure (or volume), enthalpy, and equilibrium activities of any phase in the system. As a result, the amounts of all stable phases, which reach a state of chemical equilibrium, are given as a function of temperature.[26,31] As already identified by Becidan et al.,[38] main limitations of this method are that:

- equilibrium may not be reached for all species in the real system due to kinetic constraints or low temperatures and residence times.
- no temperature and concentration gradients are taken into account.
- no diffusion paths are taken into account.
- no physical processes, for example, adsorption processes, are taken into account.
- results are dependent on the database content and reliability of the thermodynamic data.
- only elemental compositions are considered (e.g., only blank metals and no initial passive oxide layers like Cr_2O_3).

These limitations have to be carefully considered by interpreting and evaluating thermodynamic calculations and when comparing them with experimental findings. However, despite these limitations, thermodynamic equilibrium calculations are a helpful tool to identify the processes of a given system, get information about the overall stabilities, and gather information on possible or impossible pathways. They can be of great support to understanding the underlying chemical processes and complementing experimental studies.

4 | CONCLUSION

In the thermal cracking processes of postconsumer plastics, which operate at high temperatures in reducing HCl and H2S-containing atmospheres, corrosion-resistant materials are needed. To assess the performance of several high-temperature alloys in simulated environments of thermal cracking processes, corrosion mechanisms have been developed. To evaluate the overall chemistry of these complex mechanisms, which are mainly based on practical observations and kinetic considerations, a detailed thermodynamic analysis was performed. Thereby, several factors that determine the corrosion behavior of the materials in reducing HCl and H2S-containing environments have been identified:

- The type of base metal and its tendency to react with HCl and H_2S is of high importance, whereas reactions also depend on the local availabilities of the reaction partners. In the present case, chromium was identified to be the most reactive metal, followed by iron and nickel.
- Vapor pressures of volatile metal chlorides increased with rising temperature.
    - At lower temperatures, metal chlorides remain to a large extent in the corrosion layer.
    - At higher temperatures, metal chlorides, especially $FeCl_2$, are able to evaporate.
- Secondary reactions of volatile metal chlorides with H_2S, lead to the formation of metal sulfides.
- Supply of H_2S in the gas phase can determine the corrosion structure.
    - In the low-H_2S mixture at 580°C, a too small amount of H_2S is available, so that no further conversion of volatile $FeCl_2$ to FeS can take place.
    - In the mid-H_2S and the high-H_2S mixture at 580°C, enough H_2S is available, so that further conversion of volatile $FeCl_2$ to FeS can take place.
- The improved corrosion resistance of K90941 in the mid-H_2S mixture at 580°C could be explained by means of quasi-stability diagrams.
    - Partial pressures of chlorine and sulfur are close to the border between the stability of $FeCl_2$ and FeS in the mid-H_2S mixture at 580°C.
    - Competing corrosion processes between the formation of $FeCl_2$ and FeS seem to slow down the corrosive attack.

ACKNOWLEDGMENTS

The authors thank OMV Downstream GmbH for the possibility to work on this project and the support from OMV E&P. The materials were provided by Sandvik, which is gratefully acknowledged. Open Access Funding provided by KEMO - Montanuniversitat Leoben within the KUBL Agreement.

CONFLICT OF INTEREST

The authors declare no conflict of interest.

DATA AVAILABILITY STATEMENT

The data that support the findings of this study are available from the corresponding author upon reasonable request.

ORCID

Manuela Nimmervoll http://orcid.org/0000-0001-9528-228X

REFERENCES

[1] S. M. Al-Salem, P. Lettieri, J. Baeyens, *Waste Manage.* **2009**, *29*, 2625.
[2] A. K. Panda, R. K. Singh, D. K. Mishra, *Renew. Sust. Energ. Rev.* **2010**, *14*, 233.
[3] V. Goodship, *Sci. Prog.* **2007**, *90*, 245.
[4] J. Yu, L. Sun, C. Ma, H. Yao, *Waste Manage.* **2015**, *48*, 300.
[5] C. Schwalm, M. Schütze, *Mater. Corros.* **2000**, *51*, 34.
[6] A. Schmid, G. Mori, R. Haubner, M. Weil, S. Hönig, *Mater. Corros.* **2018**, *69*, 1328.
[7] D. Bramhoff, H. J. Grabke, H. P. Schmidt *The Role of Active Elements in the Oxidation Behaviour of High Temperature Metals and Alloys* ((Ed.) E. Lang), Elsevier Applied Science, London, New York **1989**, pp. 335.
[8] W. T. Bakker, *Mater. High Temp.* **1997**, *14*, 197.
[9] S. H. Lee, M. J. Castaldi presented at, *Waste-to-Energy Conf.*, Pennsylvania USA, **2008**.
[10] R. Prescott, F. H. Stott, P. Elliott, *Corr. Sci.* **1989**, *29*, 465.
[11] D. Bramhoff, H. J. Grabke, E. Reese, *Mater. Corros.* **1990**, *41*, 303.
[12] D. Bramhoff, H. J. Grabke, H. P. Schmidt, *Mater. Corros.* **1989**, *40*, 642.
[13] V. A. C. Haanappel, T. Fransen, P. J. Gellings, *High Temp. Mater. Process* **1992**, *10*, 67.
[14] H. Asteman, M. Spiegel, *Corr. Sci.* **2007**, *49*, 3626.
[15] V. A. C. Haanappel, N. Haanappel, T. Fransen, H.v Corbach, P. Gellings, *Corros.* **1992**, *48*, 812.
[16] H. P. Nielsen, F. J. Frandsen, K. Dam-Johansen, L. L. Baxter, *Prog. Energy Combust. Sci.* **2000**, *26*, 283.
[17] E. Kordzadeh, M. Bozorgmehr, *Int. J. Eng. Technol.* **2008**, *21*, 161.
[18] A. Schmid, G. Mori, E. Bucher, R. Haubner, *Oxid. Met.* **2019**, *91*, 1.
[19] A. Schmid, G. Mori, S. Strobl, R. Haubner, S. Hönig presented at, *EUROCORR 2017*, Prague, Czech Republic, 03.09.–07.09.2017, **2017**.
[20] M. Nimmervoll, G. Mori, A. Schmid, R. Haubner, S. Hönig, *Corr. Sci.* **2021**, *181*, Article 109241.
[21] M. Nimmervoll, G. Mori, E. Bucher, S. Hönig, R. Haubner, *Berg- hüttenmänn. Mon.h.* **2021**, *9*, 424.
[22] A. Schmid, G. Mori, S. Hönig, M. Weil, S. Strobl, R. Haubner, *Corr. Sci.* **2018**, *139*, 76.
[23] M. Schütze, *Mater. Sci. Technol.* **2013**, *67*, 130.
[24] M. Nimmervoll, G. Mori, E. Bucher, A. Schmid, R. Haubner, *Metals* **2021**, *11*, 1817.
[25] M. Nimmervoll, G. Mori, S. Hönig, R. Haubner, *Corr. Sci.* **2022**, *200*.
[26] G. Wedler, *Lehrbuch der Physikalischen Chemie*, Wiley-VCH Verlag GmbH, Weinheim **2004**.
[27] C. A. C. Sequeira, *High Temperature Corrosion: Fundamentals and Engineering*, 1st ed., Wiley series in corrosion, John Wiley and Sons Inc., Hoboken, New Jersey, Unites States **2019**.
[28] B. N. Popov, *Corrosion Engineering: Principles and Solved Problems*, Elsevier, Amsterdam, Netherlands **2015**.
[29] A. Schmid, G. Mori, R. Haubner, S. Hönig, *Defect Diffus. Forum* **2020**, *405*, 26.
[30] A. Schmid, G. Mori, S. Hönig, S. Strobl, R. Haubner, *Prakt. Metallog* **2019**, *56*, 457.

[31] GTT Gesellschaft für Technische Thermochemie und -physik GmbH, Software FactSage, https://gtt-technologies.de/software/factsage/, (accessed: January **2022**).
[32] R. Bender, M. Schütze, *Mater. Corros.* **2003**, *54*, 567.
[33] E. Kunze, *Korrosion und Korrosionsschutz*, Wiley-VCH Verlag GmbH, Weinheim, **2001**.
[34] P. L. Daniel, R. A. Rapp, *Advances in Corrosion Science and Technology 5*, Plenum Press, New York **1976**, pp. 55.
[35] L. L. Quill, (ed.)*The Chemistry and Metallurgy of Miscellaneous Materials: Thermodynamics*, McGraw-Hill, New York **1950**.
[36] H. Latreche, S. Doublet, M. Schütze, *Oxid. Met.* **2009**, *72*, 1.
[37] M. C. Galetz, B. Rammer, M. Schütze, *Mater. Corr.* **2015**, *66*, 1206.
[38] M. Becidan, L. Sørum, F. Frandsen, A. J. Pedersen, *Fuel* **2009**, *88*, 595.

How to cite this article: M. Nimmervoll, G. Mori, E. Bucher, S. Hönig, R. Haubner, *Mater. Corr.* **2022**, 1–25. https://doi.org/10.1002/maco.202213329